Published in final edited form as:
Dev Biol. 2010 May 1; 341(1): 154–166. doi:10.1016/j.ydbio.2010.02.019.

The Trafficking Protein Tmed2/p24β$_1$ Is Required For Morphogenesis of the Mouse Embryo and Placenta

Loydie A Jerome-Majewska[1,*], **Tala Achkar**[2], **Li Luo**[1], **Floria Lupu**[3], and **Elizabeth Lacy**[3]

[1]Department of Pediatrics, McGill University, Montreal Children's Hospital, Montreal, Quebec, Canada

[2]Department of Human Genetics, McGill University, Montreal Children's Hospital, Montreal, Quebec, Canada

[3]Developmental Biology Program, Sloan-Kettering Institute, New York, NY, USA

Abstract

During vesicular transport between the endoplasmic reticulum and the Golgi, members of the TMED/p24 protein family form hetero-oligomeric complexes that facilitate protein cargo recognition as well as vesicle budding. In addition, they regulate each other's level of expression. Despite analyses of TMED/p24 protein distribution in mammalian cells, yeast, and *C. elegans*, little is known about the role of this family in vertebrate embryogenesis. We report the presence of a single point mutation in *Tmed2/p24β$_1$* in a mutant mouse line, 99J, identified in an ENU mutagenesis screen for recessive developmental abnormalities. This mutation does not affect *Tmed2/ p24β$_1$* mRNA levels but results in loss of TMED2/p24β$_1$ protein. Prior to death at midgestation, 99J homozygous mutant embryos exhibit developmental delay, abnormal rostral-caudal elongation, randomized heart looping, and absence of the labyrinth layer of the placenta. We find that *Tmed2/ p24β$_1$* is normally expressed in tissues showing morphological defects in 99J mutant embryos and that these affected tissues lack the TMED2/p24β$_1$ oligomerization partners, TMED7/p24γ$_3$ and TMED10/p24δ$_1$. Our data reveal a requirement for TMED2/p24β$_1$ protein in the morphogenesis of the mouse embryo and placenta.

Keywords

morphogenesis; abnormal heart looping; posterior tail bud; placenta; p24; TMED; vesicular transport; ER stress

Introduction

Vesicular transport mediates molecular trafficking between the various membrane-bound compartments in a cell and thus underlies all major cellular activities. During vesicular transport members of the Transmembrane emp24 domain (TMED) or p24 protein family of trafficking proteins regulate protein-cargo selection and vesicle budding (Carney and Bowen,

*Corresponding author: Loydie A. Jerome-Majewska Research Institute of the McGill University Health Center The Montreal Children's Hospital Research Institute, Room 230 Place Toulon, 4060 Ste. Catherine St West, Montreal, Que., Canada H3Z 2Z3. Tel.514 412 4400x23279 Fax: 514 412 4331 loydie.majewska@mcgill.ca.

2004; Kaiser, 2000; Strating and Martens, 2009). Transmembrane and secreted proteins synthesized in the endoplasmic reticulum (ER) depend on vesicular transport for proper localization to the Golgi where they are further modified before being transported to their final destinations. Properly folded proteins synthesized in the ER interact with adaptors or chaperones, such as TMED/p24 proteins, which enable them to be packaged into coat protein (COP) II vesicles at ER exit sites (Bremser et al., 1999; Gurkan et al., 2006). After budding off the ER membrane, the vesicles move towards the Golgi via bulk flow or along microtubules (Cai et al., 2007). ER-resident proteins delivered to the Golgi along with cargo proteins are re-packaged into COPI vesicles and returned to the ER. Secretory cargo proteins deposited by COPII vesicles are transported through the Golgi stacks by COPI vesicles or by a process of cisternal maturation to the plasma membrane, endosomal/lysosomal system, or extracellular space.

Members of the TMED/p24 family are structurally related, sharing four distinct functional domains. A short signal sequence targets them to the ER membrane during translation; an N-terminal Golgi dynamics (GOLD) domain carries out cargo recognition; a coiled-coil domain mediates interactions between family members; and a short cytoplasmic tail contains conserved motifs for binding to coat complexes in COPI and COPII vesicles (Anantharaman and Aravind, 2002; Bethune et al., 2006; Blum et al., 1999; Bremser et al., 1999; Carney and Bowen, 2004; Dominguez et al., 1998; Goldberg, 2000; Lavoie et al., 1999; Sohn et al., 1996). Members of the TMED/p24 family fall into four subfamilies based on shared protein identity: α, β, δ and γ. Although these subfamilies are conserved in all animals and fungi, species-specific duplications and/or losses have resulted in varying numbers of genes in each TMED/p24 subfamily (Bouw et al., 2004; Carney and Bowen, 2004; Dominguez et al., 1998; Strating and Martens, 2009; Strating et al., 2009). Ten *Tmed/p24* genes are present in mammals: five in the γ subfamily, Tmed1/p24γ_1, Tmed3/p24γ_4, Tmed5/p24γ_2, Tmed6/p24γ_5, and *Tmed7/p24*γ_3; three in the α subfamily, *Tmed4/p24*α_3, *Tmed9p24*α_2 and *Tmed11/p24*α_1; one in the δ subfamily *Tmed10/p24*δ_1; and one in the β subfamily, *Tmed2/p24*β_1 (Strating et al., 2009). TMED proteins, which are herein referred to by their assigned MGI nomenclature, are reported to exist as monomers, dimers, oligomers or hetero-oligomers (Barr et al., 2001; Carney and Bowen, 2004; Jenne et al., 2002; Luo et al., 2007; Marzioch et al., 1999). According to other experimental evidence, hetero-oligomers comprising one member of each of the four subfamilies form the functional units required for vesicular transport (Blum et al., 1999; Marzioch et al., 1999)

Genetic and biochemical experiments reveal that interactions between TMED proteins regulate their stability: knockdown or deletion of one TMED protein led to decrease or loss of expression of TMED proteins from different subfamilies (Blum et al., 1999; Carney and Bowen, 2004; Denzel et al., 2000; Fullekrug et al., 1999; Marzioch et al., 1999; Takida et al., 2008; Wen and Greenwald, 1999). A null mutation in *Tmed10* resulted in developmental arrest before blastocyst formation and decreased expression of two interacting TMED proteins, TMED9 and TMED3, in livers of heterozygous mice (Denzel et al., 2000). In both yeast and mammalian cell lines, TMED2, the sole member of the β subfamily, is found in a complex containing TMED10 and/or TMED7, as well as TMED9 and it is required for their stability (Barr et al., 2001; Fullekrug et al., 1999; Jenne et al., 2002; Marzioch et al., 1999).

Members of the TMED family localize to membranes of the ER, ERGIC (endoplasmic reticulum-Golgi intermediate compartment) and cis-Golgi as well as to COPI and COPII vesicles. Biochemical and genetic experiments demonstrate that TMED proteins bind to both COPI and COPII proteins and likely function in anterograde and retrograde transport between the ER and the Golgi (Bethune et al., 2006; Bremser et al., 1999; Dominguez et al., 1998; Goldberg, 2000). In yeast, mutations of the *Tmed2* homolog, emp24, result in delayed maturation of Gas1p, a GPI-anchored protein, and defective transport of invertase, a soluble

secreted protein (Marzioch et al., 1999; Muniz et al., 2000). In mammalian cells, reduction of TMED10 levels by RNAi delayed trafficking of GPI anchored proteins to the plasma membrane (Takida et al., 2008). Thus, TMED proteins appear to be required in both yeast and mammalian cells specifically for movement of GPI anchored proteins to the plasma membrane.

In addition to impairing anterograde protein trafficking, mutations in TMED proteins trigger the ER stress-associated unfolded protein response. Loss of TMED proteins in yeast activates splicing of XBP1 pre-mRNA, leading to synthesis of the transcription factor that regulates the unfolded protein response. Loss of TMED also resulted in increased expression and abnormal secretion of Kar2, the yeast orthologue of *Hspa5/Grp78*, an ER resident chaperone belonging to the heat shock protein 70 (HSP 70) family (Belden and Barlowe, 2001). Similarly, In mammalian cells knockdown of TMED4 led to upregulation of HSP 70 and to decreased apoptosis (Hwang et al., 2008). In *Drosophila*, mutation of Logjam, the *Tmed3* homolog, caused activation of the NF-κB pathway without the associated splicing of *Xbp1* (Boltz and Carney, 2008). Thus, TMED proteins may modulate multiple cellular stress pathways.

In *C. elegans*, a screen for suppressors of *lin-12/Glp* alleles encoding Notch receptors with reduced activity, identified mutations in the C.elegans *Tmed2* homolog, *sel-9* (Wen and Greenwald, 1999). All of the *lin-12/Glp* alleles suppressed by *sel-9* mutations carried missense mutations in their extracellular domain. Whereas in wild type strains altered Notch proteins accumulate within the cell, in the *sel-9* mutants altered Notch assembled at the cell membrane where it was functional (Wen and Greenwald, 1999). Trafficking of wild type Notch/Glp did not require *sel-9*; thus Tmed2 likely functions in quality control, specifically selecting defective Notch/Glp as cargo. Studies in primary rat astrocytes and human endothelial kidney cells found that TMED2 interacts with PAR-2, a G protein-coupled receptor that is activated at the plasma membrane by protease cleavage (Luo et al., 2007). Downstream signaling triggered by PAR-2 activation released TMED2-bound PAR-2, freeing it to traffic from the Golgi to the plasma membrane. In this case, TMED2-cargo selectivity appears to regulate post-Golgi protein trafficking.

Here we report the identification of a null allele of *Tmed2* in an N-ethyl N-nitrousurea (ENU) screen for recessive mutations perturbing the morphology of the developing mouse embryo. The mutation was discovered in a mouse line designated 99J and the mutant allele named $Tmed2^{99J}$ (herein referred to as 99J). *99J* homozygous mutant embryos exhibit developmental delay by E8.5, fail to undergo embryonic turning, and display posterior truncations, abnormal heart looping, and absence of the labyrinth layer of the placenta. The mutant embryos are reabsorbed by mid-gestation. Using positional cloning and sequencing we determined that the $Tmed2^{99J}$ allele carries a G:C to T:A transversion in the first exon, generating an alanine to glutamic acid substitution in the TMED2 signal sequence, blocking the production of any TMED2 protein. Failure to complement a gene trap allele of *Tmed2* confirmed that the mutation in $Tmed2^{99J}$ underlies the phenotypic defects. The levels of TMED7 and TMED10 protein were decreased in 99J heterozygous embryos and absent in the homozygous mutants embryo, revealing that TMED2 regulates the stability of these γ and δ subfamily members. The mid-gestation defects of $Tmed2^{99J}$ suggest that the cargos selected and trafficked by TMED2 participate in the morphogenetic processes of early development.

Materials and Methods

1. Mouse strains

The 99J line was generated by ENU mutagenesis of C57BL/6J mice (Anderson, 2000; Garcia-Garcia and Anderson, 2003; Kasarskis et al., 1998) and backcrossed to C3HeB/FeJ females. The PST809 cell line, with insertion of a gene trap cassette in the 3rd intron of *Tmed2*, $Tmed2^{GT}$, was identified on ENSEMBL (http://baygenomics.ucsf.edu/). The insertion was

sequenced and verified before injection into C57 blastocysts. The chimeric offspring were bred to C57BL/Crc females and heterozygous F1 (C57/129) mice were bred to 99J heterozygous carriers for complementation analysis. CD1 (Charles Rivers, Canada) females mated to CD1 male were used to generate embryos for wholemount in situ hybridization. All mouse breedings and manipulations were performed in accordance with the Canadian Council on Animal Research. To generate embryos, females were placed with a male overnight and checked for the presence of a vaginal plug in the morning. The day that a plug was detected was considered embryonic day (E) 0.5. Mice and embryos from the 99J ENU line were genotyped by PCR with primers to D5MIT65 and D5MIT213. Mice and embryos from the Pst809 gene-trap line were genotyped with primers from JaxMice that recognize the LacZ gene or with primers which were designed to distinguish the wild type *Tmed2* allele from the gene trapped allele. Primers *Tmed2*In4F and *Tmed2*In4R amplified the wild type *Tmed2* allele, and primers *Tmed2*In4F and Genetrap1R amplified the genetrap allele.

*Tmed2*In4F: *AAGTGCACAGCTGAGTGGT*

*Tmed2*In4R: *CACAGTGTCTGACCCCCTTT*

Genetrap1R: *AAGGGTCTTTGAGCACCAGA*

2. Mapping of the 99J mutation

The mutation was mapped using linkage to flanking simple sequence length polymorphism (SSLP) markers from the MIT database or new markers that we generated (http://mouse.ski.mskcc.org/). Exons, splice site acceptors and splice site donors of 35 genes in the 99J minimal region were sequenced at the McGill Genome Center. Genomic DNA from 99J homozygous mutant embryos (n=6), carrier mice (n=2), and two wild type strains C3H/HeJ (n=1) and C57bL/6J mice (n=1) were analyzed with SeqMan II (DNASTAR).

3. RT- PCR

RNA isolation was performed according to standard Trizol (Invitrogen) protocol. The RNA was treated with DNAse prior to reverse transcription reaction. Reverse transcription was done using the Superscript III RT kit (Invitrogen). The *Tmed2*F and *Tmed2*R primers were designed to amplify wild type *Tmed2*, the *Tmed2*E3F and *Genetrap*R primers were used to amplify the *g*enetrap mutation in the PST809 cell line, and two primers were used to amplify *Gapdh*:

*Tmed2*E1F: 5’-GATGGGCCTCATCTTCGAG-3’

*Tmed2*E4R: 5’-ACCAAAGGACCACTCTGCTG-3’

*Tmed2*E3F: CAATGACAGCCGTAAAGCAC

*Genetrap*R: GTGATCCAGGACTGGGAAGA

*Gapdh*F: 5’-ATGACATCAAGAAGGTCCTG-3’

*Gapdh*R: 5’-CATACCAGGAAATGAGCTTG-3’

4. In situ hybridization, immunohistochemistry

Wholemount in situ hybridization was performed on E6.5, E7.5, E8.5, E9.5, E10.5 and E11.5 embryos and placentas. The yolk sacs were collected for genotyping and the placentas and embryos were fixed in PFA, dehydrated and processed for wholemount in situ hybridization according to standard protocols (Wilkinson et al., 1990). Wholemount embryos were examined on a Leica stereomicroscope MZFL III (Leica, Germany) microscope and photographed using a SPOTcam (RT-Slider, USA) camera after wholemount.

For section in situ hybridization and immunohistochemistry, E8.5, E9.5 and E10.5 deciduas were fixed in PFA, embedded in paraffin, and sectioned at 7 μm. Embryonic tissue was scraped off the slides and used to genotype the embryos. Slides containing 99J homozygous mutant embryos and normal controls were used for in situ hybridization or immunohistochemistry. In situ hybridization was performed as described by Neubuser et al. (1995).

We generated two *Tmed2* probes. The exon1 specific probe was made by PCR amplification of exon 1 of the *Tmed2* gene from E8.5 decidual cDNA using primers that were designed to be complementary to Ensembl sequence ENSMUSG000000293902 (Forward primer: CGAGGAGTGCTTCTTCGAG; Reverse primer: TCCCGGACTTCCATGTACTC). The full length probe was generated by PCR amplification of exon 1 – 4 of the *Tmed2* gene from E9.5 embryonic cDNA using primers (Forward primer: GATGGGCCTCATCTTCGAG and Reverse primer: ACCAAAGGACCACTCTGCTG). PCR amplicons of the correct size were subcloned using the dual promoter TA cloning kit (Invitrogen). The *Tmed2*-TA clones were sequenced on the ABI Prism 310 Genetic analyzer (Perkin Elmer) before probe generation. To generate digoxigenin labeled probe *Tmed2*-TA constructs were linearized and transcribed using the T7 promoter or Sp6 promoters to generate antisense and sense probes, respectively. Since the exon1 specific probe reported the same expression pattern as the full length probe, the two probes were used interchangeably. RNA probes for *Mash2, Gcm*1, *Esx1, Pl1* and *Tpbp* were kind gifts from Dr. J. Cross (U. Calgary).

Immunohistochemistry was performed according to standard protocols (2003). Antibodies against VCAM 1 (Santa Cruz) and α4 integrin (Santa Cruz) were used at 1:100 dilutions for immunohistochemistry on sections of E8.5 normal and 99J homozygous mutant embryos. Experimental slides were imaged on an Axiovert Imager. Z1 (Zeiss, Germany) and pictures were captured on an Axiocam MrC5 (Zeiss, Germany).

5. Western blot analysis

Individual E9.5 and E10.5 embryos were dissected out of their extra-embryonic membranes and either lysed immediately or flash frozen at -80°C before western blot analysis. Groups of wild type (2 embryos), 99J heterozygous (2 embryos) or 99J homozygous mutant embryos (4 embryos) were homogenized with a syringe and lysed in buffer containing: 50 mM Tris, 150 mM NaCl, 1% NP-40, 1.5 mM Mgcl2, 10% Glycerol, 1 mM EDTA, 25 mM NaF and 1 mM Na_3VO_4. After protein quantification, 20 μg of protein was separated on a 10% SDS-PAGE gel and electroblotted onto a PVDF Nitrocellulose membrane (Bio-Rad). The blots were blocked in 5% milk and incubated with primary antibodies recognizing the cytosolic tails of TMED2, TMED7, TMED9, TMED10 (Denzel et al., 2000), HSPA5/GRP78 (Abcam, MA), GRP94 (Abcam, MA) and GAPDH (Abcam, MA) diluted in blocking buffer. The blots were washed and incubated with HRP-conjugated goat anti-rabbit IgG (Jackson ImmunoResearch) secondary antibody. The blots were developed with an ECL plus chemiluminescence kit (Amersham).

6. ER Stress

To determine if the unfolded protein response pathway is activated in 99J homozygous mutant embryos we designed primers for RT-PCR to amplify the *Xbp*1 mRNA (Forward primer: GATCCTGACGAGGTTCCAGA and Reverse primer: GGTCCCCACTGACAGAGAAA). The PCR product was digested with *Pst*1 restriction enzyme which yields two bands (240 bp and 110 bp) in the absence of ER stress and a single 350 bp band in the presence of ER stress. Primary embryonic fibroblast cells (PMEFs) were cultured in the presence or absence of thapsigargin (Sigma), according to standard protocols (Leclerc and Rozen, 2008).

Results

Developmental delay in 99J homozygous mutant embryos

The ENU mouse line 99J was identified in a phenotypic screen for recessive mutations that disrupt embryonic morphology at E9.5 (Garcia-Garcia et al., 2005). 99J homozygous mutant embryos displayed several phenotypic abnormalities at midgestation (Fig. 1) and failed to survive embryogenesis (Table 1). To determine the developmental stage at which 99J homozygous mutant embryos first exhibited morphological defects, litters from 99J heterozygous intercrosses were examined between E7.5 and E12.5. At E7.5, 99J homozygous mutant embryos were indistinguishable from their normal littermates and were present at the predicted Mendelian ratio (Table 1). Starting at E8.5, 99J homozygous embryos appeared developmentally delayed relative to wild type and 99J heterozygous embryos. At this stage, expression of *Sonic Hedghehog (Shh)* a morphogen that is normally expressed in the node and midline of normal E8.5 embryos was also altered. In fact, *Shh* was only expressed in the head process of 99J homozygous embryos (n=2; Fig. 1A, B), similar to the characterized expression domain of this gene at E7.5 (Bai et al., 2002). Furthermore, E8.5 mutants also contained fewer somites than normal littermates (0-4 pairs of somites; Table 2). By E9.5, 0-10 somite pairs had formed in 99J homozygous mutants, whereas 20-22 somite pairs had formed in their wild type littermates (Fig. 1C; Table 2). 99J homozygous mutant embryos presented a number of additional abnormalities, including a failure to turn, an open neural tube, a small, irregularly shaped tail-bud and a bulbous allantois (Fig. 1D). The heart in 10 % of E9.5 99J homozygous mutant embryos (n=5/48) lacked detectable beating, indicating that some 99J mutants arrested before E9.5 (Table 1).

99J homozygous mutant embryos exhibited discordant development along the rostral-caudal body axis and abnormal heart formation (Table 1; Fig. 1). The rostral half of an E10.5 99J homozygous mutant embryo resembled that of a normal E9.5 embryo; it contained closed headfolds, otic and optic vesicles with morphological signs of differentiation, and forelimb buds (Fig. 1D, E). In contrast, the caudal end of an E10.5 mutant embryo was reduced in size and consisted primarily of a small, malformed tail bud that was devoid of tissue (Fig. 1E).. In normal E8.5 embryos the linear heart-tube loops in a rightward direction to ensure proper positioning of the future ventricles and atria. Only 23.1% of E10.5 99J homozygous mutant embryos (n = 3/13) showed rightward heart looping, while 53.8% showed irregular looping (n = 7/13; Fig 1G, I) and the heart failed to loop in the remaining 23.1% (n= 3/13; Fig 1H) (Table 1B). Abnormal heart looping is associated with delayed or absent expression of the TGF-β family member, *Nodal*, at the node (Krebs et al., 2003). However, *in situ* hybridization revealed *Nodal* expression in the node of 99J homozygous mutants analyzed between E8.5 and E9.5 (n=4, data not shown). Thus, abnormal heart looping was not due to a failure to initiate *Nodal* expression at the node. No homozygous mutant offspring were recovered at E11.5 and E12.5 (Table 1).

Abnormal placental development in 99J homozygous mutant embryos

Embryonic survival after E10.5 requires a functional placenta (Watson and Cross, 2005); therefore we examined the development of extraembryonic regions in 99J homozygous mutant embryos to determine if placental defects contributed to the observed embryonic lethality. Chorioallantoic attachment, the joining of the chorion to the tip of the allantois, marks the morphological appearance of the developing placenta at E8.5 (Cross et al., 2003). Analysis of whole mount embryos at E8.5 revealed that 99J mutants failed to undergo chorioallantoic attachment. However, immunohistochemistry detected normal expression in both mutant and wild type embryos of two proteins known to mediate chorioallantoic attachment: VCAM1, in the allantois and its receptor α4 integrin in the chorion (Kwee et al., 1995; Yang et al., 1995) (data not shown). Thus, the normal distribution of VCAM1 and α4 integrin does not require

TMED2; delayed chorioallantoic attachment in the 99J mutant likely reflects an overall developmental delay.

Following spreading of the allantois over the surface of the chorion and subsequent chorioallantoic attachment, branching morphogenesis to form the villi of the labyrinth layer of the placenta is initiated at E9.0 (Fig. 2A, C & E). The labyrinth layer, which mediates nutrient and waste exchange between the maternal and fetal environments, consists of allantois-derived fetal blood vessels, as well as maternal blood sinusoids embedded in a trilaminar trophoblast (Rossant and Cross, 2001; Simmons et al., 2008). Fetal blood vessels can be distinguished from maternal sinusoids on the basis of red blood cell morphology: embryonic red blood cells are nucleated, while maternal red blood cells lack nuclei. Due to developmental delay in the 99J homozygote, we examined mutant embryos at E10.5 to determine whether they had initiated formation of the labyrinth layer. The placenta in normal E10.5 embryos exhibited the expected histological giant cell, spongiotrophoblast, and labyrinth layers (Fig. 2C, E). Although the allantois had begun to spread over the surface of the chorion in 99J homozygous mutant embryos, it showed no evidence of invagination into the chorion to form the labyrinth layer (Fig. 2D, F). Unlike wild type embryos, 99J homozygous mutants contained fetal blood vessels only in the allantois and at the boundary between the allantois and the chorion. The observed absence of the labyrinth layer in the 99J homozygous mutant embryo, and thus of a mechanism for nutrient-waste exchange between the fetal and maternal blood supplies, likely underlies their death at midgestation.

The initiation of branching morphogenesis and the ensuing population of the forming villi with allantois- derived vessels depend on proper expression of the transcription factor *Gcm1* in the chorion (Anson-Cartwright et al., 2000; Schreiber et al., 2000). In situ hybridization detected comparable levels of *Gcm1* expression in the chorionic plate of normal and 99J homozygous mutant embryos at E8.5 (Fig 3A, B), indicating appropriate differentiation of chorionic ectoderm in 99J. However, only a subset of 99J homozygous mutant embryos between E9.5 and E10.5 expressed *Gcm1* (n=2/4). In those embryos, *Gcm1* expression was restricted to a small region of the chorionic plate (Fig 3D), while in similarly staged wild type embryos, *Gcm1* expression was distributed throughout the chorionic component of the labyrinth layer (Fig. 3C). These data suggest that lack of labyrinth layer formation in the 99J mutant does not result from deficient or inappropriate *Gcm1* expression.

Formation of a functional placenta also depends on the differentiation of other trophectoderm-derived cell layers, such as giant cells and the spongiotrophoblast. Histological examination identified giant cells in the placenta of E9.5 mutant embryos (Fig. 2D, F). In situ hybridization to *placental lactogen (Pl)1*, a marker for trophoblast giant cells (Simmons and Cross, 2005) detected *Pl1* expression in a layer of cells immediately below the maternal decidua in both E9.5 normal and 99J homozygous mutant embryos, confirming the presence of giant cells in mutant placentas (Fig 3E, F). Similarly, *in situ* hybridization to *Trophoblast specific protein (Tpbp) alpha*, a gene expression marker for spongiotrophoblast cells (Simmons and Cross, 2005), found *Tpbpa* transcripts in the placenta of both normal and 99J homozygous mutant embryos at E9.5, suggesting that spongiotrophoblast cells differentiate appropriately in the 99J mutant (Fig. 3G, H). However, whereas the *Tpbpa* positive cells resided immediately above the labyrinth layer in the placenta from normal embryos, they were located immediately adjacent to the apparently undifferentiated chorion in the placenta from 99J homozygous mutant embryos (Fig 3 G-H). These data suggest that the 99J mutant might be specifically impaired in the formation of the labyrinth layer. On the other hand, since distinct differentiated trophoblast cell types arise from precursors present in the E8.5 chorion, prior to elaboration of the labyrinth layer (Simmons et al., 2008), the absence of this layer in the 99J mutant might simply reflect developmental delay.

Identification of a point mutation in *Tmed2* in Line 99J

We initially mapped the 99J mutation to mouse chromosome 5 within a 2 Mb interval flanked by MIT markers D5 MIT65 and D5 MIT139. An evaluation of the 35 genes within this interval revealed that targeted deletion/knockout of four of these genes did not generate embryonic lethality, eliminating them from further consideration as the mutated gene in line 99J (Akhmanova et al., 2005; Hughes et al., 2004; Hyun et al., 2004; Lu et al., 2001; Okada et al., 2002; Reiter and Skarnes, 2006). To further reduce the list of potential candidates, we examined the expression of the remaining 31 genes in the 99J critical interval by RT-PCR. Transcripts from three genes were not detected in either normal or 99J homozygous mutant embryos at E9.5, removing them as viable candidates for the 99J mutation (Table 3). Whole mount *in situ* hybridization for 24 of the now 28 candidate genes determined that three of them *Tmed2*, *Eif2b1*, and *D5Bwg0834e*- were expressed in both the embryo and placenta at E9.5 (Table 3). Parallel experiments to sequence the coding regions and donor and acceptor splice sites of all 35 genes in the 99J interval identified a single point mutation, a G:C to T:A transversion, in the first exon of *Tmed2* in 99J homozygous mutant (n=4) and 99J heterozygous (n=3) embryos (Fig. 4A). The G:C to T:A transversion produced a missense mutation that replaced a highly conserved alanine residue in the signal peptide sequence of TMED2 with glutamic acid (A13E) (Fig. 4A). Mutations in the hydrophobic core of signal sequences are associated with loss or decreased protein levels due to abnormal translocation into the ER and/or protein stability (Karaplis et al., 1995; Kendall et al., 1990; Lanza et al., 2002; Nicchitta et al., 2005; Pidasheva et al., 2005; Symoens et al., 2009; Wiren et al., 1989). Thus, we anticipated that the A13E substitution would result in decreased expression or loss of TMED2 protein. Consistent with this prediction, *Tmed2* transcripts were present at relatively normal levels in mutant embryos at E9.5 (Fig. 4B), whereas levels of TMED2 protein were reduced in 99J heterozygotes and undetectable in 99J homozygotes at E9.5-E10.5 (Fig. 4C and data not shown).

To confirm that the $Tmed2^{99J}$ allele underlies the recessive midgestation lethality in line 99J, we generated a second mutant allele of *Tmed2* for complementation analysis. Using the PST 809 ES cell clone (BayGenomics), we generated a line of mice carrying a gene trap allele of *Tmed2*, $Tmed2^{GT}$. The gene trap is inserted into the third intron of *Tmed2* (Fig. 5A) where it promotes the synthesis of a fusion protein between the first 71 amino acids of TMED2, including the cargo recognition domain (GOLD), and β-galactosidase. A similarly truncated TMED2 protein has been shown to function as a dominant negative mutant *in vitro* (Luo et al., 2007). Examination of E10.5 embryos produced from matings between $Tmed2^{GT/+}$ females and $Tmed2^{99J/+}$ males demonstrated a lack of complementation between the gene trap and ENU alleles of *Tmed2*. Recovered trans-heterozygous $Tmed2^{GT/99J}$ embryos morphologically resembled $Tmed2^{99J/99J}$ mutant embryos: they displayed a reduced size compared to normal littermates, abnormal heart looping and a small, irregularly shaped tail bud (Fig. 5C and data not shown).

Tmed2 expression during embryonic and placental development

To establish the temporal pattern of *Tmed2* expression during mouse development, we performed RT-PCR on wild type embryos recovered at different times of gestation between E3.5 and E10.5. Robust and continuous transcription of *Tmed2* was observed from implantation at E4.5 through the onset of organogenesis at E10.5 (Fig 6). We investigated the spatial distribution of *Tmed2* transcription in E5.5 – E10.5 embryos and placentas by *in situ* hybridization. Two distinct cDNA probes (see Materials and Methods) revealed specific and identical patterns of *Tmed2* expression between E5.5 and E10.5 (Fig. 7 and S1). In E5.5 embryos, we detected uniform *Tmed2* expression throughout the embryonic and extraembryonic components of the egg cylinder (Fig. S1A.). In more developmentally advanced E5.5 embryos *Tmed2* expression was highest in the extraembryonic regions, including the ectoplacental cone, parietal endoderm, and visceral endoderm (Fig. S1B-D).

Nonetheless, *Tmed2* expression was still detected in the embryonic ectoderm of all embryos analyzed at this stage (Fig. S1A-D).

The initial ubiquitous expression of *Tmed2* became spatially restricted by E6.5. During gastrulation *Tmed2* was expressed in a very dynamic pattern. E6.5 embryos expressed *Tmed2* at the highest levels in ectoplacental cone and extraembryonic ectoderm and at lower levels in visceral endoderm and epiblast (Fig. 7A and Fig. S1E– H)). In late headfold stage E7.5 embryos *Tmed2* was found in ectoplacental cone, amnion, anterior neural folds and underlying head mesoderm as well as in the proximal region of the primitive streak (Fig 7C-D and S1I-L). At E8.5 *Tmed2* was broadly expressed throughout the embryo, including a region around the node, the neural folds, and allantois (Fig. 7E). In situ hybridization to sections of E8.5 embryos revealed *Tmed2* in lateral plate mesoderm, the somites, the tailbud, the heart and aortic arteries (Fig 7E, S1M-P). Overall *Tmed2* was expressed in derivatives of all three germ layers - ectoderm, mesoderm and endoderm - although it was at higher levels in the mesoderm and its derivatives. In the endoderm, *Tmed2* expression was detected in the foregut but not in the midgut and hindgut (Fig. S1, M-P). As the embryo completed turning between E8.5-E9.0, the highest levels of *Tmed2* were found in the forebrain, otic vesicle, first pharyngeal arch and tail bud (Fig 7E, F). E9.5, embryos expressed *Tmed2* in the forebrain, otic and optic vesicles, liver anlage, limb buds, neural tube, and tail bud (Fig 7G). At E10.5 *Tmed2* was broadly expressed in most embryonic structures, including the ventricles of the heart (data not shown).

Tmed2 expression was maintained throughout placental development. E6.5 and E7.5 embryos expressed *Tmed2* in extraembryonic ectoderm and chorion, respectively (Fig. 7A-D), while E8.5 embryos expressed *Tmed2* in the allantois, chorionic plate and giant cells of the now forming placenta (Fig. 8A). At E9.5 the placenta exhibited *Tmed2* expression in the labyrinth, spongiotrophoblast and giant cell layers, but not in the attached allantois (Fig. 8B). By E10.5 *Tmed2* expression was detected in a subset of giant cells (Fig. 8C), in trophoblast cells surrounding the maternal sinusoids, and in fetal blood vessels in the placenta (Fig. 8D).

Reduced protein levels of TMED7 and TMED10 in 99J homozygous mutant embryos

Previous studies revealed interdependence among TMED proteins for regulation of their expression levels (Jenne et al., 2002; Luo et al., 2007). Therefore, we performed western blot analysis to assess whether the levels of TMED proteins known to interact with TMED2, TMED7, TMED9 and TMED10 (Jenne et al., 2002; Marzioch et al., 1999), were altered in 99J mutants. We found that the levels of TMED7, TMED9 and TMED10 were reduced in 99J heterozygous embryos at E9.5 and E10.5 (Fig. 9 A-C). While expression levels of TMED9 were further reduced in 99J homozygous mutant embryos at E9.5-E10.5 (Fig. 9A), expression of TMED7 and TMED10 was undetectable in mutant embryos at these same stages. However, mRNA levels for *Tmed7*, *Tmed9*, and *Tmed10* did not vary between normal and 99J mutant embryos at E9.5-E10.5 (Fig. 5B and data not shown). These data suggest that loss of TMED2 directly affects the stability of TMED7, TMED9 and TMED10 at the protein level.

Failure to activate the unfolded protein response pathway in *Tmed2*$^{99J/99J}$ mutant embryos

In yeast, deletion of the *Tmed2* and *Tmed10* homologs activates the unfolded protein response pathway. The mutant yeast strains upregulate expression of the ER chaperone protein HSPA5/GRP78 and also splicing of *Hac-1* RNA, encoding a functional homolog of the transcription factor XBP1 (Belden and Barlowe, 2001; Kuznetsov et al., 1997; Rose et al., 1989; Yoshida et al., 1998; Yoshida et al., 2001). Therefore, we hypothesized that the 99J mutant embryos would display increased secretion of HSPA5/GRP78 and splicing of *Xbp*1 RNA. However, we failed to detect abnormal activation of the unfolded protein response pathway in 99J mutant embryos. Expression of the ER chaperone proteins HSPA5/GRP78 and HSP90β1/GRP94 did not increase in E10.5 99J mutant embryos (Fig. 10A). In addition, expression and splicing of

the *Xbp*1 transcript appeared unaltered in 99J mutants compared to wild type embryos (Fig 10B). In control assays, efficient splicing of *Xbp*1 was detected in PMEFs after treatment with the ER stress-inducing agent, thapsigargin (Fig 10B). Thus, our data suggest that the loss of TMED2, TMED7, and TMED10 does not activate the unfolded protein response in mouse embryos.

Discussion

Tmed2 is expressed during embryonic and placental development

TMED proteins are highly conserved in eukaryotes and are implicated in vesicular transport. We report that *Tmed2* is expressed in embryonic and extraembryonic tissues of the developing mouse embryo and is required for morphogenesis of both the embryo and the placenta. *Tmed2* mutant embryos fail to form the labyrinth layer of the placenta and die by midgestation, revealing a previously uncharacterized requirement for vesicular transport in placental development. Minimal information exists on the expression of *Tmed* genes in mammalian tissues and our study represents the first effort to systematically document expression of a *Tmed* gene during embryonic development. Of potential significance to TMED function, our study reveals that *Tmed2*, the single member of the β-subfamily, is expressed tissue-specifically during embryonic development.

It has been proposed that TMED family members form hetero-oligomers, consisting of one member of each subfamily, to facilitate formation of COPI and COPII vesicles (Marzioch et al., 1999). While *Tmed2* is expressed at all stages of postimplantation development analyzed in this study, it assumes a tissue-specific expression pattern by E6.5, suggesting a temporally and spatially restricted role in vesicle-trafficking.

Tmed2 is required for labyrinth layer formation

Tmed2 mutant embryos exhibit developmental delay and are smaller than their normal littermates. These defects could reflect, in part, abnormal and/or reduced vesicular transport in the yolk sac, a structure that expresses *Tmed2* and that mediates nutrient uptake by the early post-implantation embryo (Conway et al., 2003). By E10.5, the nutritional requirements of the embryo can no longer be met exclusively by the yolk sac and the continuation of development requires a functional placenta (Conway et al., 2003; Rossant and Cross, 2001). The labyrinth layer of the placenta, which is composed of fetal blood vessels and maternal blood spaces, now takes over as the primary site for nutrient and waste exchange between the growing fetus and its maternal environment (Watson and Cross, 2005). Mutants that fail to form this labyrinth layer arrest at mid-gestation, likely due to nutritional deficiency (Watson and Cross, 2005). We propose that *Tmed2* homozygous mutant embryos die at mid-gestation because of impaired labyrinth layer development.

Chorioallantoic attachment initiates the formation of the labyrinth layer. Downs and Gardner (1995) suggest that chorioallantoic attachment occurs in at least three steps: contact between the allantois and the posterior end of the chorion, translocation of the allantois to the center of the chorion, and invasion of the allantois into the chorion. In *Tmed2* mutant embryos, the allantois contacts but does not invade the chorion. Failure of allantois cell invasion into the chorion results in a weak attachment between the two tissues. Moreover, the absence of a labyrinth layer in *Tmed2* mutants suggests that allantois cell invasion may function as the trigger for reorganization of chorion cells into the labyrinth layer. Failure of allantois invasion into the chorion of *Tmed2* mutant embryos might be a non-specific effect of developmental delay. Alternatively, it may point to the requirement for the delivery of specific cargo proteins to the allantois-chorion interface by TMED2-mediated trafficking.

TMED2 is required for normal expression of TMED7 and TMED10

A large number of studies have shown that the expression of individual TMED proteins is interdependent (Bouw et al., 2004; Denzel et al., 2000; Jenne et al., 2002; Luo et al., 2007; Marzioch et al., 1999; Muniz et al., 2000). Our own studies provide further support for this interdependency; however, the significance and requirement for this remain unclear. We found that loss of TMED2 results in loss of TMED7 and TMED10 expression and a decrease in expression of TMED9. Since mutant embryos lacking TMED10 arrest and die prior to implantation at E4.5 (Denzel et al., 2000), whereas *Tmed2* mutants survive up to E10.5, TMED10 expression and function must be independent of stable, zygotic expression of *Tmed2* in the pre-implantation mouse embryo. These findings indicate that individual members of the TMED protein family are essential for distinct stage and tissue-specific functions during development.

Vesicular transport proteins are required for normal morphogenesis

A large family of molecular motor proteins consisting of cytoplasmic dyneins, axonal dyneins and kinesins are required for transport in the cytoplasm and cilia; reviewed in (Hirokawa and Noda, 2008). In addition, two subunits of the COPII coat complex interact with Dynactin1, the cofactor of the dynein molecular motor (Watson et al., 2005), suggesting that vesicular transport by COPII proteins may require normal expression and function of molecular motor proteins. Since TMED2 also interacts with COPII coat complexes (Bethune et al., 2006; Bremser et al., 1999; Dominguez et al., 1998) transport of TMED2 cargo proteins from the endoplasmic reticulum may be mediated by microtubule based motors. Embryos with mutations in *Dynactin1* as well as several molecular motors -*mD2lic*, *Kif3A*, and *Kif3B* - either arrest before E8.0 or exhibit a number of morphological phenotypes, including developmental delay, abnormal heart looping and rostro-caudal truncations, suggesting that these molecules are required for normal development and morphogenesis (Lai et al., 2007; Marszalek et al., 1999; Nonaka et al., 1998; Rana et al., 2004; Takeda et al., 1999). Thus it will be important to explore whether these molecular motors are required for trafficking of TMED2 cargo proteins.

TMED2-Protein trafficking, quality control and post-Golgi exocytosis

In yeast, deletion of *Tmed2* results in increased secretion of the ER stress associated protein HSPA5/GRP78 and upregulation and splicing of the pre-mRNA encoding XBP1, a transcriptional regulator of the ER stress pathway (Belden and Barlowe, 2001). Hence, we expected that 99J homozygous mutant embryos would exhibit increased HSPA5/GRP78 protein levels. However, we did not detect increased levels of HSPA5/GRP78 or HSP90β1/GRP94, indicating that *Tmed2* mutations do not contribute to increased ER stress in the developing mouse embryo. Furthermore, we did not find increased expression or splicing of *Xbp1* (Yoshida et al., 2001). Our data are consistent with a report by Boltz and Carney (2008) reporting that the loss of TMED proteins in *Drosophila* does not trigger *Xbp*1 upregulation and splicing; rather, they observed activation of the NF-κB pathway. Activation of the NF-κB pathway independently of unfolded protein response has been reported in mammalian cells as well (Davies et al., 2009; Pahl et al., 1996); therefore future studies will examine this pathway in *Tmed2* homozygous mutant embryos.

TMED2 interacts with COPII vesicles (Bethune et al., 2006; Dominguez et al., 1998; Majoul et al., 2001), which *in vitro* form a cage around newly synthesized proteins and regulate their anterograde transport from the ER. In addition, two studies, one in *C. elegans* (Wen and Greenwald, 1999), and one in an astrocyte cell line (Luo et al., 2007), suggest that TMED2 may function at other steps in the secretory pathway, possibly in COPI vesicles within the Golgi compartments.

COPII and COPI vesicles, and by extension members of the TMED protein family, play fundamental roles in the intracellular transport of proteins through the secretory pathway. Moreover, cell-cell interactions, as well as the execution of most cell behaviors, depend on the secretory pathway to deliver intact, functional proteins to their appropriate intracellular and extracellular compartments. Consequently the defects displayed by *Tmed2*-deficient embryos potentially reflect the defective transport and localization of one or several developmentally critical proteins. Recently an examination of genetic interactions between mutant alleles exhibiting similar phenotypes led to the demonstration that Sec24b, a core component of COPII vesicles, regulates planar cell polarity in the neural tube through selective sorting of Vangl2 (Merte et al.). A similar approach, combined with the generation of a conditional *Tmed2* allele, will be applied to identify proteins that specifically rely on TMED2 for vesicular transport during the gastrulation stages of mouse development.

Supplementary Material

Refer to Web version on PubMed Central for supplementary material.

Acknowledgments

We would like to thank Dr. Kathryn Anderson for the 99J ENU line, Dr. John Bergeron and Tommy Nilsson for Tmed antibodies, Dr. Roberta Rivi and Yulan Hu for help with the mice. We thank Dr. Aimee Ryan, Dr. Virginia Papaioannou, Dr. Tomoko Watanabe and Michelle Collins for critical reading of the manuscript. We are grateful to the McGill Genome Center for sequencing the *Tmed2* mutation and the Montreal Transgenic Core for generating the Pst809 genetrap allele. LAM was funded by NSERC and CIHR operating grants and FRSQ. LAJM and LL are members of the Research Institute of the McGill University Health Centre, which is supported in part by the FRSQ.

References

Manipulating the mouse embryo : a laboratory manual. Cold Spring Harbor Laboratory Press; Cold Spring Harbor, N.Y.: 2003.

Akhmanova A, Mausset-Bonnefont AL, van Cappellen W, Keijzer N, Hoogenraad CC, Stepanova T, Drabek K, van der Wees J, Mommaas M, Onderwater J, et al. The microtubule plus-end-tracking protein CLIP-170 associates with the spermatid manchette and is essential for spermatogenesis. Genes Dev 2005;19:2501–15. [PubMed: 16230537]

Anantharaman V, Aravind L. The GOLD domain, a novel protein module involved in Golgi function and secretion. Genome Biol 2002;3 research0023.

Anderson KV. Finding the genes that direct mammalian development : ENU mutagenesis in the mouse. Trends Genet 2000;16:99–102. [PubMed: 10689347]

Anson-Cartwright L, Dawson K, Holmyard D, Fisher SJ, Lazzarini RA, Cross JC. The glial cells missing-1 protein is essential for branching morphogenesis in the chorioallantoic placenta. Nat Genet 2000;25:311–4. [PubMed: 10888880]

Bai CB, Auerbach W, Lee JS, Stephen D, Joyner AL. Gli2, but not Gli1, is required for initial Shh signaling and ectopic activation of the Shh pathway. Development 2002;129:4753–61. [PubMed: 12361967]

Barr FA, Preisinger C, Kopajtich R, Korner R. Golgi matrix proteins interact with p24 cargo receptors and aid their efficient retention in the Golgi apparatus. J Cell Biol 2001;155:885–91. [PubMed: 11739402]

Belden WJ, Barlowe C. Deletion of yeast p24 genes activates the unfolded protein response. Mol Biol Cell 2001;12:957–69. [PubMed: 11294899]

Bethune J, Kol M, Hoffmann J, Reckmann I, Brugger B, Wieland F. Coatomer, the coat protein of COPI transport vesicles, discriminates endoplasmic reticulum residents from p24 proteins. Mol Cell Biol 2006;26:8011–21. [PubMed: 16940185]

Blum R, Pfeiffer F, Feick P, Nastainczyk W, Kohler B, Schafer KH, Schulz I. Intracellular localization and in vivo trafficking of p24A and p23. J Cell Sci 1999;112(Pt 4):537–48. [PubMed: 9914165]

Boltz KA, Carney GE. Loss of p24 function in Drosophila melanogaster causes a stress response and increased levels of NF-kappaB-regulated gene products. BMC Genomics 2008;9:212. [PubMed: 18466616]

Bouw G, Van Huizen R, Jansen EJ, Martens GJ. A cell-specific transgenic approach in Xenopus reveals the importance of a functional p24 system for a secretory cell. Mol Biol Cell 2004;15:1244–53. [PubMed: 14699062]

Bremser M, Nickel W, Schweikert M, Ravazzola M, Amherdt M, Hughes CA, Sollner TH, Rothman JE, Wieland FT. Coupling of coat assembly and vesicle budding to packaging of putative cargo receptors. Cell 1999;96:495–506. [PubMed: 10052452]

Cai H, Reinisch K, Ferro-Novick S. Coats, tethers, Rabs, and SNAREs work together to mediate the intracellular destination of a transport vesicle. Dev Cell 2007;12:671–82. [PubMed: 17488620]

Carney GE, Bowen NJ. p24 proteins, intracellular trafficking, and behavior: Drosophila melanogaster provides insights and opportunities. Biol Cell 2004;96:271–8. [PubMed: 15145531]

Conway SJ, Kruzynska-Frejtag A, Kneer PL, Machnicki M, Koushik SV. What cardiovascular defect does my prenatal mouse mutant have, and why? Genesis 2003;35:1–21. [PubMed: 12481294]

Cross JC, Simmons DG, Watson ED. Chorioallantoic morphogenesis and formation of the placental villous tree. Ann N Y Acad Sci 2003;995:84–93. [PubMed: 12814941]

Davies MJ, Miranda E, Roussel BD, Kaufman RJ, Marciniak SJ, Lomas DA. Neuroserpin polymers activate NF-kappaB by a calcium signaling pathway that is independent of the unfolded protein response. J Biol Chem 2009;284:18202–9. [PubMed: 19423713]

Denzel A, Otto F, Girod A, Pepperkok R, Watson R, Rosewell I, Bergeron JJ, Solari RC, Owen MJ. The p24 family member p23 is required for early embryonic development. Curr Biol 2000;10:55–8. [PubMed: 10660306]

Dominguez M, Dejgaard K, Fullekrug J, Dahan S, Fazel A, Paccaud JP, Thomas DY, Bergeron JJ, Nilsson T. gp25L/emp24/p24 protein family members of the cis-Golgi network bind both COP I and II coatomer. J Cell Biol 1998;140:751–65. [PubMed: 9472029]

Fullekrug J, Suganuma T, Tang BL, Hong W, Storrie B, Nilsson T. Localization and recycling of gp27 (hp24gamma3): complex formation with other p24 family members. Mol Biol Cell 1999;10:1939–55. [PubMed: 10359607]

Garcia-Garcia MJ, Anderson KV. Essential role of glycosaminoglycans in Fgf signaling during mouse gastrulation. Cell 2003;114:727–37. [PubMed: 14505572]

Garcia-Garcia MJ, Eggenschwiler JT, Caspary T, Alcorn HL, Wyler MR, Huangfu D, Rakeman AS, Lee JD, Feinberg EH, Timmer JR, et al. Analysis of mouse embryonic patterning and morphogenesis by forward genetics. Proc Natl Acad Sci U S A 2005;102:5913–9. [PubMed: 15755804]

Goldberg J. Decoding of sorting signals by coatomer through a GTPase switch in the COPI coat complex. Cell 2000;100:671–9. [PubMed: 10761932]

Gurkan C, Stagg SM, Lapointe P, Balch WE. The COPII cage: unifying principles of vesicle coat assembly. Nat Rev Mol Cell Biol 2006;7:727–38. [PubMed: 16990852]

Hirokawa N, Noda Y. Intracellular transport and kinesin superfamily proteins, KIFs: structure, function, and dynamics. Physiol Rev 2008;88:1089–118. [PubMed: 18626067]

Hughes M, Dobric N, Scott IC, Su L, Starovic M, St-Pierre B, Egan SE, Kingdom JC, Cross JC. The Hand1, Stra13 and Gcm1 transcription factors override FGF signaling to promote terminal differentiation of trophoblast stem cells. Dev Biol 2004;271:26–37. [PubMed: 15196947]

Hwang SO, Boswell SA, Seo JS, Lee SW. Novel oxidative stress-responsive gene ERS25 functions as a regulator of the heat-shock and cell death response. J Biol Chem 2008;283:13063–9. [PubMed: 18326488]

Hyun TS, Li L, Oravecz-Wilson KI, Bradley SV, Provot MM, Munaco AJ, Mizukami IF, Sun H, Ross TS. Hip1-related mutant mice grow and develop normally but have accelerated spinal abnormalities and dwarfism in the absence of HIP1. Mol Cell Biol 2004;24:4329–40. [PubMed: 15121852]

Jenne N, Frey K, Brugger B, Wieland FT. Oligomeric state and stoichiometry of p24 proteins in the early secretory pathway. J Biol Chem 2002;277:46504–11. [PubMed: 12237308]

Kaiser C. Thinking about p24 proteins and how transport vesicles select their cargo. Proc Natl Acad Sci U S A 2000;97:3783–5. [PubMed: 10760248]

Karaplis AC, Lim SK, Baba H, Arnold A, Kronenberg HM. Inefficient membrane targeting, translocation, and proteolytic processing by signal peptidase of a mutant preproparathyroid hormone protein. J Biol Chem 1995;270:1629–35. [PubMed: 7829495]

Kasarskis A, Manova K, Anderson KV. A phenotype-based screen for embryonic lethal mutations in the mouse. Proc Natl Acad Sci U S A 1998;95:7485–90. [PubMed: 9636176]

Kendall DA, Doud SK, Kaiser ET. A comparative analysis of single- and multiple-residue substitutions in the alkaline phosphatase signal peptide. Biopolymers 1990;29:139–47. [PubMed: 2183883]

Krebs LT, Iwai N, Nonaka S, Welsh IC, Lan Y, Jiang R, Saijoh Y, O'Brien TP, Hamada H, Gridley T. Notch signaling regulates left-right asymmetry determination by inducing Nodal expression. Genes Dev 2003;17:1207–12. [PubMed: 12730124]

Kuznetsov G, Chen LB, Nigam SK. Multiple molecular chaperones complex with misfolded large oligomeric glycoproteins in the endoplasmic reticulum. J Biol Chem 1997;272:3057–63. [PubMed: 9006956]

Kwee L, Baldwin HS, Shen HM, Stewart CL, Buck C, Buck CA, Labow MA. Defective development of the embryonic and extraembryonic circulatory systems in vascular cell adhesion molecule (VCAM-1) deficient mice. Development 1995;121:489–503. [PubMed: 7539357]

Lai C, Lin X, Chandran J, Shim H, Yang WJ, Cai H. The G59S mutation in p150(glued) causes dysfunction of dynactin in mice. J Neurosci 2007;27:13982–90. [PubMed: 18094236]

Lanza F, De La Salle C, Baas MJ, Schwartz A, Boval B, Cazenave JP, Caen JP. A Leu7Pro mutation in the signal peptide of platelet glycoprotein (GP)IX in a case of Bernard-Soulier syndrome abolishes surface expression of the GPIb-V-IX complex. Br J Haematol 2002;118:260–6. [PubMed: 12100158]

Lavoie C, Paiement J, Dominguez M, Roy L, Dahan S, Gushue JN, Bergeron JJ. Roles for alpha(2)p24 and COPI in endoplasmic reticulum cargo exit site formation. J Cell Biol 1999;146:285–99. [PubMed: 10427085]

Leclerc D, Rozen R. Endoplasmic reticulum stress increases the expression of methylenetetrahydrofolate reductase through the IRE1 transducer. J Biol Chem 2008;283:3151–60. [PubMed: 18065414]

Lu C, Peng YW, Shang J, Pawlyk BS, Yu F, Li T. The mammalian retinal degeneration B2 gene is not required for photoreceptor function and survival. Neuroscience 2001;107:35–41. [PubMed: 11744244]

Luo W, Wang Y, Reiser G. p24A, a type I transmembrane protein, controls ARF1-dependent resensitization of protease-activated receptor-2 by influence on receptor trafficking. J Biol Chem. 2007

Majoul I, Straub M, Hell SW, Duden R, Soling HD. KDEL-cargo regulates interactions between proteins involved in COPI vesicle traffic: measurements in living cells using FRET. Dev Cell 2001;1:139–53. [PubMed: 11703931]

Marszalek JR, Ruiz-Lozano P, Roberts E, Chien KR, Goldstein LS. Situs inversus and embryonic ciliary morphogenesis defects in mouse mutants lacking the KIF3A subunit of kinesin-II. Proc Natl Acad Sci U S A 1999;96:5043–8. [PubMed: 10220415]

Marzioch M, Henthorn DC, Herrmann JM, Wilson R, Thomas DY, Bergeron JJ, Solari RC, Rowley A. Erp1p and Erp2p, partners for Emp24p and Erv25p in a yeast p24 complex. Mol Biol Cell 1999;10:1923–38. [PubMed: 10359606]

Merte J, Jensen D, Wright K, Sarsfield S, Wang Y, Schekman R, Ginty DD. Sec24b selectively sorts Vangl2 to regulate planar cell polarity during neural tube closure. Nat Cell Biol 12:41–6. sup pp 1-8. [PubMed: 19966784]

Muniz M, Nuoffer C, Hauri HP, Riezman H. The Emp24 complex recruits a specific cargo molecule into endoplasmic reticulum-derived vesicles. J Cell Biol 2000;148:925–30. [PubMed: 10704443]

Neubuser A, Koseki H, Balling R. Characterization and developmental expression of Pax9, a paired-box-containing gene related to Pax1. Dev Biol 1995;170:701–16. [PubMed: 7649395]

Nicchitta CV, Lerner RS, Stephens SB, Dodd RD, Pyhtila B. Pathways for compartmentalizing protein synthesis in eukaryotic cells: the template-partitioning model. Biochem Cell Biol 2005;83:687–95. [PubMed: 16333319]

Nonaka S, Tanaka Y, Okada Y, Takeda S, Harada A, Kanai Y, Kido M, Hirokawa N. Randomization of left-right asymmetry due to loss of nodal cilia generating leftward flow of extraembryonic fluid in mice lacking KIF3B motor protein. Cell 1998;95:829–37. [PubMed: 9865700]

Okada H, Suh WK, Jin J, Woo M, Du C, Elia A, Duncan GS, Wakeham A, Itie A, Lowe SW, et al. Generation and characterization of Smac/DIABLO-deficient mice. Mol Cell Biol 2002;22:3509–17. [PubMed: 11971981]

Pahl HL, Sester M, Burgert HG, Baeuerle PA. Activation of transcription factor NF-kappaB by the adenovirus E3/19K protein requires its ER retention. J Cell Biol 1996;132:511–22. [PubMed: 8647884]

Pidasheva S, Canaff L, Simonds WF, Marx SJ, Hendy GN. Impaired cotranslational processing of the calcium-sensing receptor due to signal peptide missense mutations in familial hypocalciuric hypercalcemia. Hum Mol Genet 2005;14:1679–90. [PubMed: 15879434]

Rana AA, Barbera JP, Rodriguez TA, Lynch D, Hirst E, Smith JC, Beddington RS. Targeted deletion of the novel cytoplasmic dynein mD2LIC disrupts the embryonic organiser, formation of the body axes and specification of ventral cell fates. Development 2004;131:4999–5007. [PubMed: 15371312]

Reiter JF, Skarnes WC. Tectonic, a novel regulator of the Hedgehog pathway required for both activation and inhibition. Genes Dev 2006;20:22–7. [PubMed: 16357211]

Rose MD, Misra LM, Vogel JP. KAR2, a karyogamy gene, is the yeast homolog of the mammalian BiP/GRP78 gene. Cell 1989;57:1211–21. [PubMed: 2661018]

Rossant J, Cross JC. Placental development: lessons from mouse mutants. Nat Rev Genet 2001;2:538–48. [PubMed: 11433360]

Schreiber J, Riethmacher-Sonnenberg E, Riethmacher D, Tuerk EE, Enderich J, Bosl MR, Wegner M. Placental failure in mice lacking the mammalian homolog of glial cells missing, GCMa. Mol Cell Biol 2000;20:2466–74. [PubMed: 10713170]

Simmons DG, Cross JC. Determinants of trophoblast lineage and cell subtype specification in the mouse placenta. Dev Biol 2005;284:12–24. [PubMed: 15963972]

Simmons DG, Natale DR, Begay V, Hughes M, Leutz A, Cross JC. Early patterning of the chorion leads to the trilaminar trophoblast cell structure in the placental labyrinth. Development 2008;135:2083–91. [PubMed: 18448564]

Sohn K, Orci L, Ravazzola M, Amherdt M, Bremser M, Lottspeich F, Fiedler K, Helms JB, Wieland FT. A major transmembrane protein of Golgi-derived COPI-coated vesicles involved in coatomer binding. J Cell Biol 1996;135:1239–48. [PubMed: 8947548]

Strating JR, Martens GJ. The p24 family and selective transport processes at the ER-Golgi interface. Biol Cell 2009;101:495–509. [PubMed: 19566487]

Strating JR, van Bakel NH, Leunissen JA, Martens GJ. A comprehensive overview of the vertebrate p24 family: identification of a novel tissue-specifically expressed member. Mol Biol Evol 2009;26:1707–14. [PubMed: 19429673]

Symoens S, Malfait F, Renard M, Andre J, Hausser I, Loeys B, Coucke P, De Paepe A. COL5A1 signal peptide mutations interfere with protein secretion and cause classic Ehlers-Danlos syndrome. Hum Mutat 2009;30:E395–403. [PubMed: 18972565]

Takeda S, Yonekawa Y, Tanaka Y, Okada Y, Nonaka S, Hirokawa N. Left-right asymmetry and kinesin superfamily protein KIF3A: new insights in determination of laterality and mesoderm induction by kif3A-/- mice analysis. J Cell Biol 1999;145:825–36. [PubMed: 10330409]

Takida S, Maeda Y, Kinoshita T. Mammalian GPI-anchored proteins require p24 proteins for their efficient transport from the ER to the plasma membrane. Biochem J 2008;409:555–62. [PubMed: 17927562]

Watson ED, Cross JC. Development of structures and transport functions in the mouse placenta. Physiology (Bethesda) 2005;20:180–93. [PubMed: 15888575]

Watson P, Forster R, Palmer KJ, Pepperkok R, Stephens DJ. Coupling of ER exit to microtubules through direct interaction of COPII with dynactin. Nat Cell Biol 2005;7:48–55. [PubMed: 15580264]

Wen C, Greenwald I. p24 proteins and quality control of LIN-12 and GLP-1 trafficking in Caenorhabditis elegans. J Cell Biol 1999;145:1165–75. [PubMed: 10366590]

Wilkinson DG, Bhatt S, Herrmann BG. Expression pattern of the mouse T gene and its role in mesoderm formation. Nature 1990;343:657–9. [PubMed: 1689462]

Wiren KM, Ivashkiv L, Ma P, Freeman MW, Potts JT Jr. Kronenberg HM. Mutations in signal sequence cleavage domain of preproparathyroid hormone alter protein translocation, signal sequence cleavage, and membrane-binding properties. Mol Endocrinol 1989;3:240–50. [PubMed: 2710131]

Yang JT, Rayburn H, Hynes RO. Cell adhesion events mediated by alpha 4 integrins are essential in placental and cardiac development. Development 1995;121:549–60. [PubMed: 7539359]

Yoshida H, Haze K, Yanagi H, Yura T, Mori K. Identification of the cis-acting endoplasmic reticulum stress response element responsible for transcriptional induction of mammalian glucose-regulated proteins. Involvement of basic leucine zipper transcription factors. J Biol Chem 1998;273:33741–9. [PubMed: 9837962]

Yoshida H, Matsui T, Yamamoto A, Okada T, Mori K. XBP1 mRNA is induced by ATF6 and spliced by IRE1 in response to ER stress to produce a highly active transcription factor. Cell 2001;107:881–91. [PubMed: 11779464]

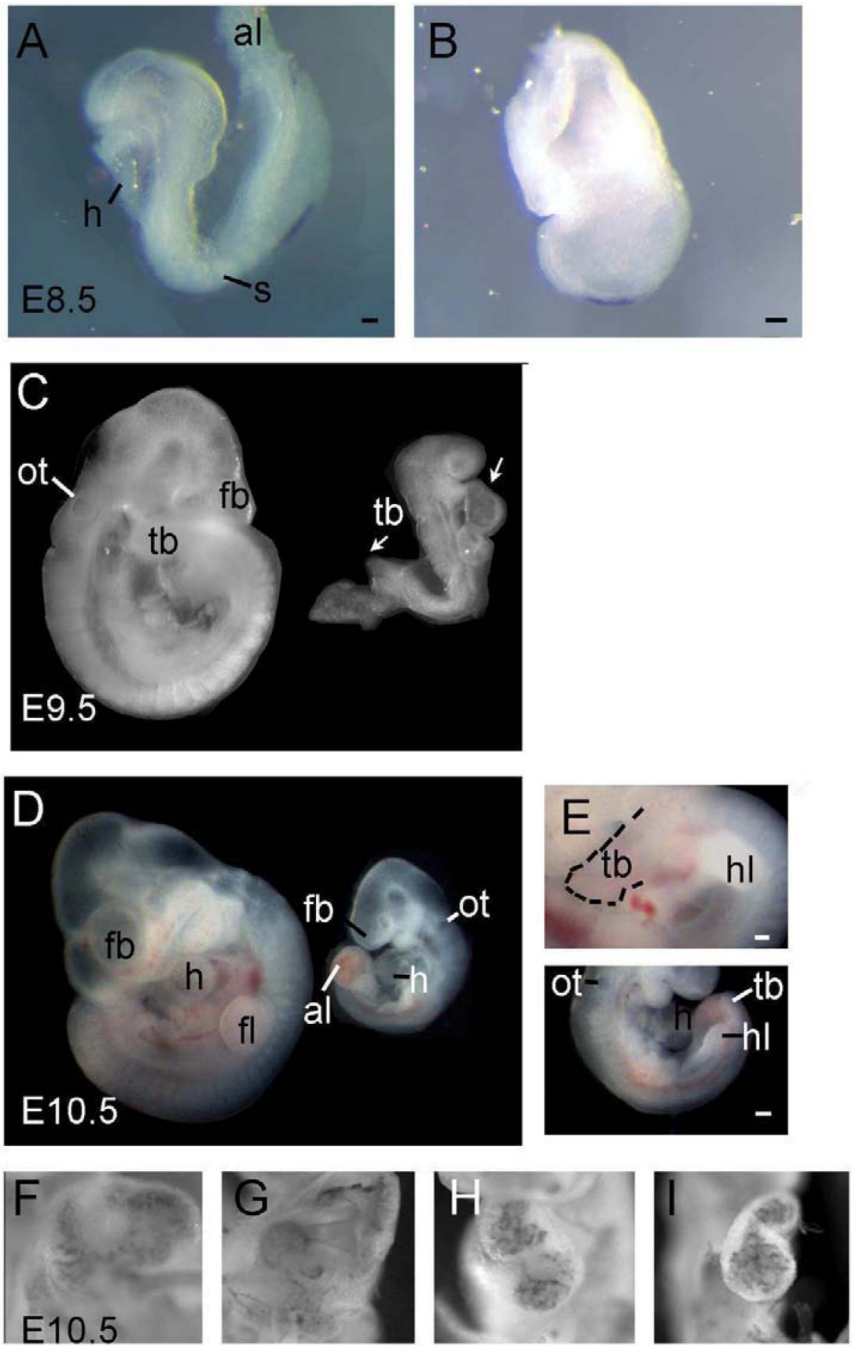

Figure 1. Morphology of normal and 99J homozygous mutant embryos

99J homozygous mutant embryos exhibit developmental delay, posterior truncations and abnormal heart looping. (**A, B)** Representative E8.5 embryos after wholemount in situ hybridization to detect expression of *shh*; the wild type embryo (**A)** has five somite pairs (s), heart (h) and allantois (al) and expresses *shh* in the node and midline. The homozygous mutant embryo (**B)** resembles an egg cylinder, has no somites and expresses *shh* in the head process. (**C**) While the wild type E9.5 embryo (left) has turned and contains 20+ somites, its 99J mutant littermate (right) remains unturned with small abnormal somites and shows a small, pointy tail bud (tb) and an unlooped heart tube (arrow). (**D)** An E10.5 99J mutant embryo (right) has undergone turning but remains developmentally delayed compared to a wild type littermate

(left). The mutant embryo possesses a forming forebrain (fb), otic vesicle (ot), heart (h) and a balled allantois (al). (**E)** A lateral (right side) view of the normal (top) and mutant (bottom) embryos shown in panel D. Hind limb (hl) buds are present in both embryos; however the posterior of the 99J homozygous mutant embryo is truncated and the tail bud (tb) is abnormal. **(F)** Rigthward heart looping in a normal embryo. **(G, I)** 99J homozygous mutant embryos exhibit leftward and unlooped hearts (h). Abbreviations: normal embryo (N); otic vesicle (ot), forelimb bud (fl), hind limb bud (hl), Tail bud (tb). Scale bar in A & B = 50 μm.

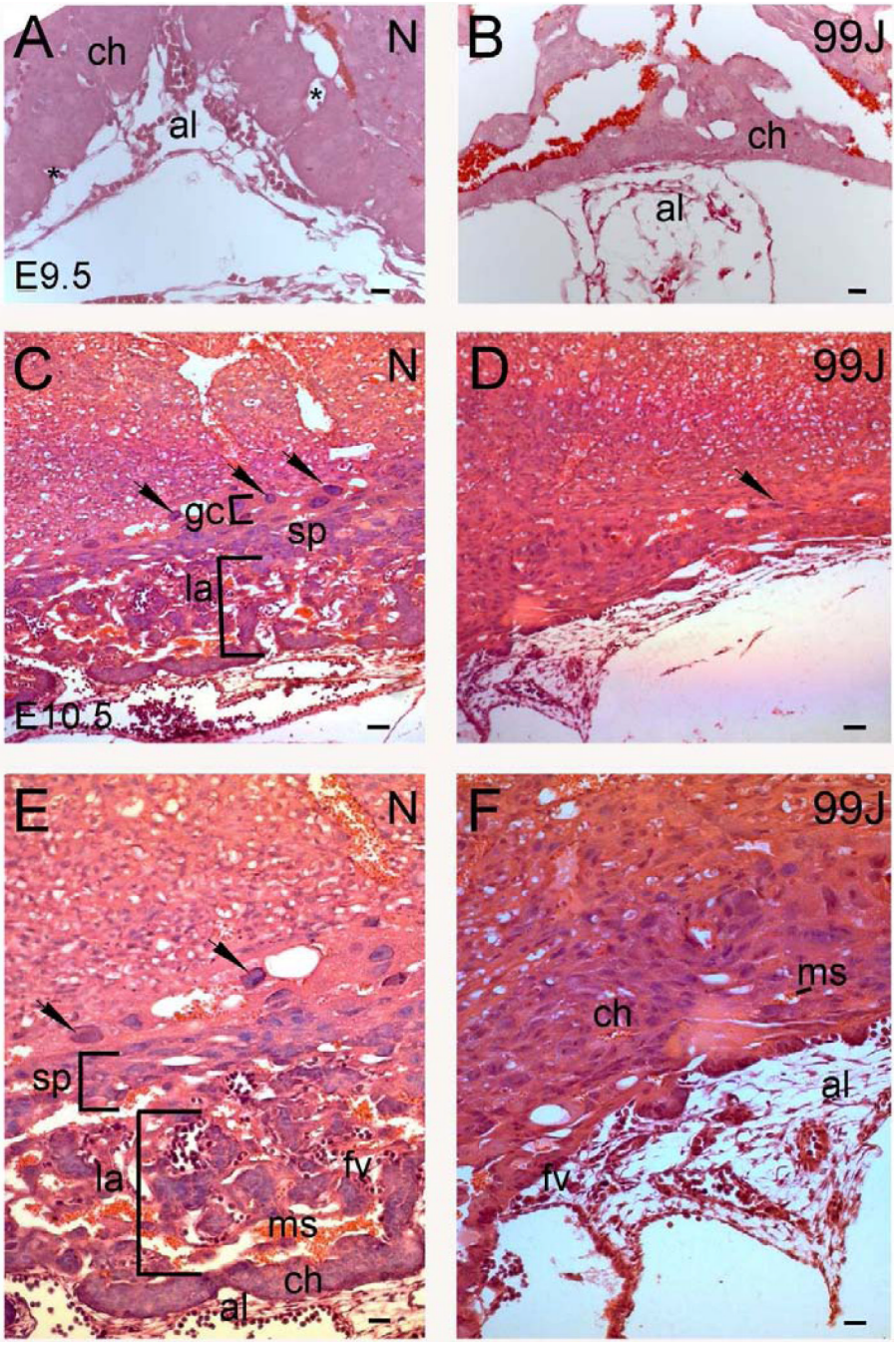

Figure 2. Chorioallantoic attachment and branching morphogenesis in placentas from normal and 99J homozygous mutant embryos

(**A**) A normal E9.5 embryo shows a fan shaped allantois (al) attached to the chorion (ch) and fetal blood vessels (asterisks *) forming in the chorion. (**B**) A representative image of a 99J homozygous mutant embryo with limited contact between the allantois and chorion. (**C, E**) A normal E10.5 placenta with distinguishable giant cells (gc, arrowheads), spongiotrophoblast (sp) and labyrinth (la) layers. (**E)** A higher magnification view of the placenta shown in C; maternal blood sinusoids (ms) with enucleated blood cells lie in close proximity to the fetal blood vessels (fv) with the nucleated blood cells (**D, F**) In E10.5 99J homozygous mutant embryos the allantois has spread along the surface of the chorion. Giant cells (arrowhead) but

no distinct spongiotrophoblast and labyrinth layers are present in the chorionic plate (ch). (**F**) A higher magnification image of the placenta shown in D, maternal blood sinusoids are visible in the chorion, but fetal blood vessels are detectable only in the allantois and at the junction between the chorion and allantois. Scale bars = 100 μm (**A, B**), 50 μm (**C-D**) and 20 μm (**E, F).**

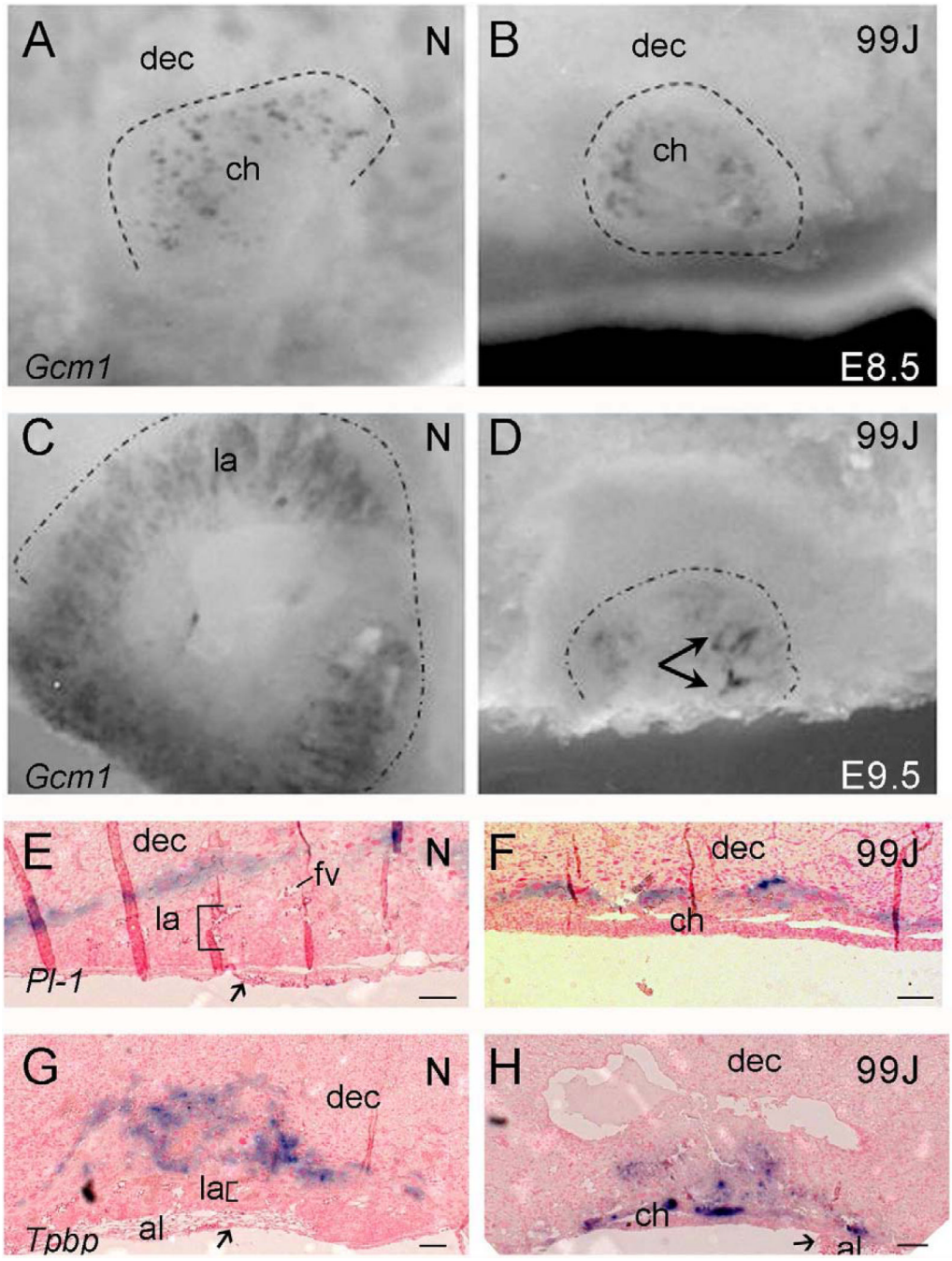

Figure 3. Molecular analysis of placental development in normal and 99J homozygous mutant embryos

Representative images of wild type and mutant deciduas (**A, B)** and placentas (**C - H)** after wholemount *in situ* hybridization to an antisense *Gcm1* riboprobe (**A-D**) and *in situ* hybridization of histological sections to antisense *Pl1* (**E, F**) and *Tpbp* (**G, H)** riboprobes. At E8.5, *Gcm1* is expressed in the chorionic trophoblast cells of normal (**A**) and 99J homozygous mutant embryos (**B**). (**C**) At E9.5 *Gcm1* is expressed in the developing labyrinth layer of the placenta in a normal embryo. (**D**) *Gcm1* expression is present but reduced and regionally restricted (arrows) in the placenta of an E9.5 99J homozygous mutant. The dotted lines in panels A- D delineate the chorionic plate. **(E**) A normal placenta at E9.5 showing expression

of the giant cell marker *Pl1*, above the forming labyrinth (la) layer. (**F**) Although a labyrinth layer did not form in the placenta of an E9.5 99J mutant embryo, the expression pattern of *Pl1* is similar to that observed in the normal embryo. (**G**) Expression of *4331*/*Tpbpa* in spongiotrophoblast cells below the giant cell layer and above the labyrinth layer (la) in a representative E9.5 normal embryo. (**H**) *Tpbpa* positive cells reside immediately above the chorionic layer in the placenta of an E9.5 99J mutant embryo. The arrows point to attached and apposed allantois in normal (**E, G**) and 99J homozygous mutant embryos (**H**), respectively. Abbreviations: fetal blood vessels (fv), chorion (ch), decidua (dec). Scale bars = 100 μm.

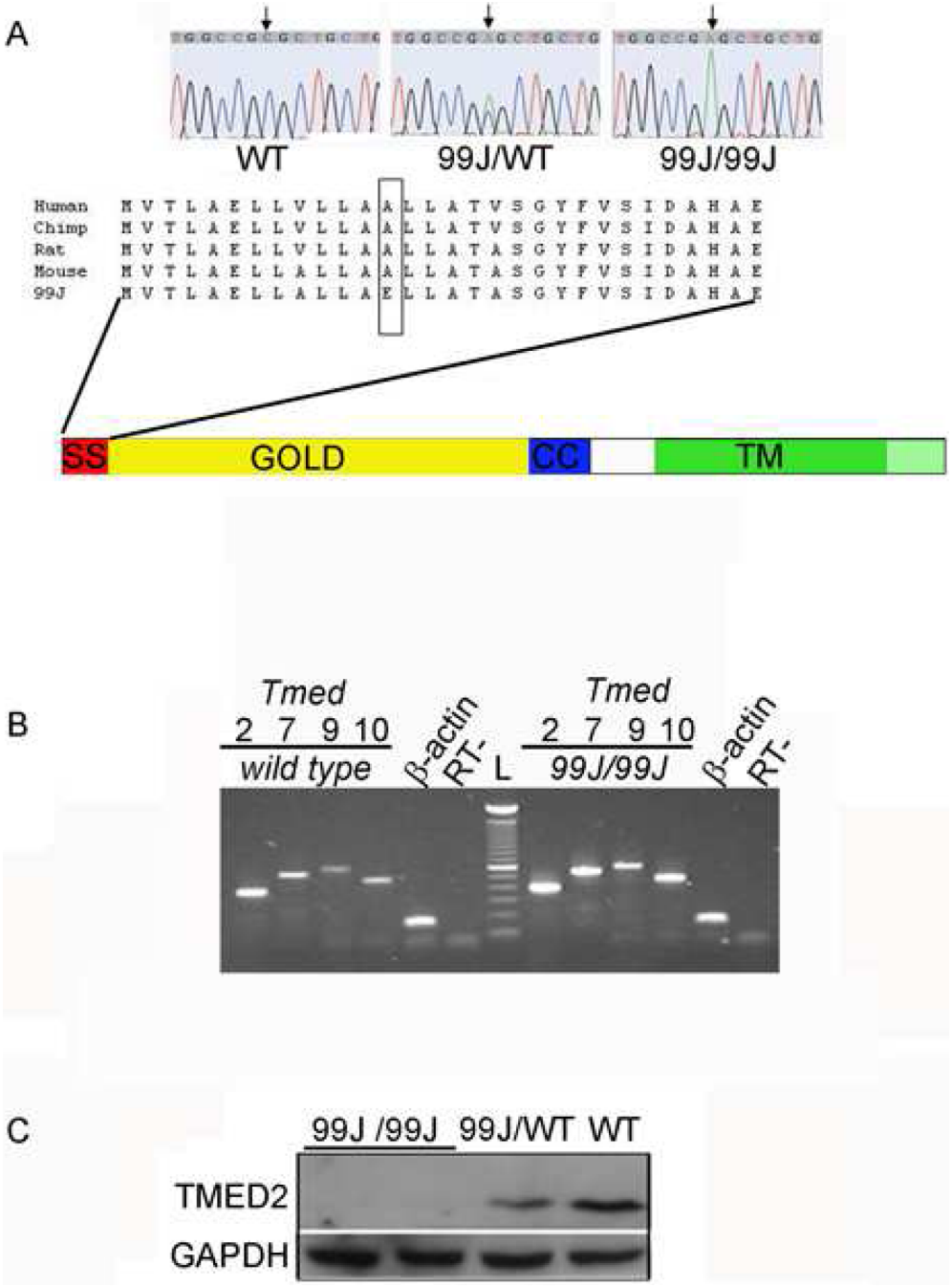

Figure 4. The 99J ENU line has a mutation in *Tmed2*

(A) The 99J mutation, a C to A transversion in the first exon of *Tmed2*, results in substitution of an alanine residue with a glutamic acid in the highly conserved signal sequence. **(B)** RT-PCR analysis revealed normal expression of *Tmed2*, *Tmed7*, *Tmed9* and *Tmed10* in wild type and 99J homozygous mutant embryos. A 100 bp marker, the β-actin positive control and RT- controls are also shown. **(C)** A representative Western blot shows TMED2 protein is present in protein lysates from E9.5 wild type and 99J heterozygous embryos. TMED2 is not detected in two different pools of four 99J homozygous mutant embryos (99J/99J). GAPDH was used as a loading control.

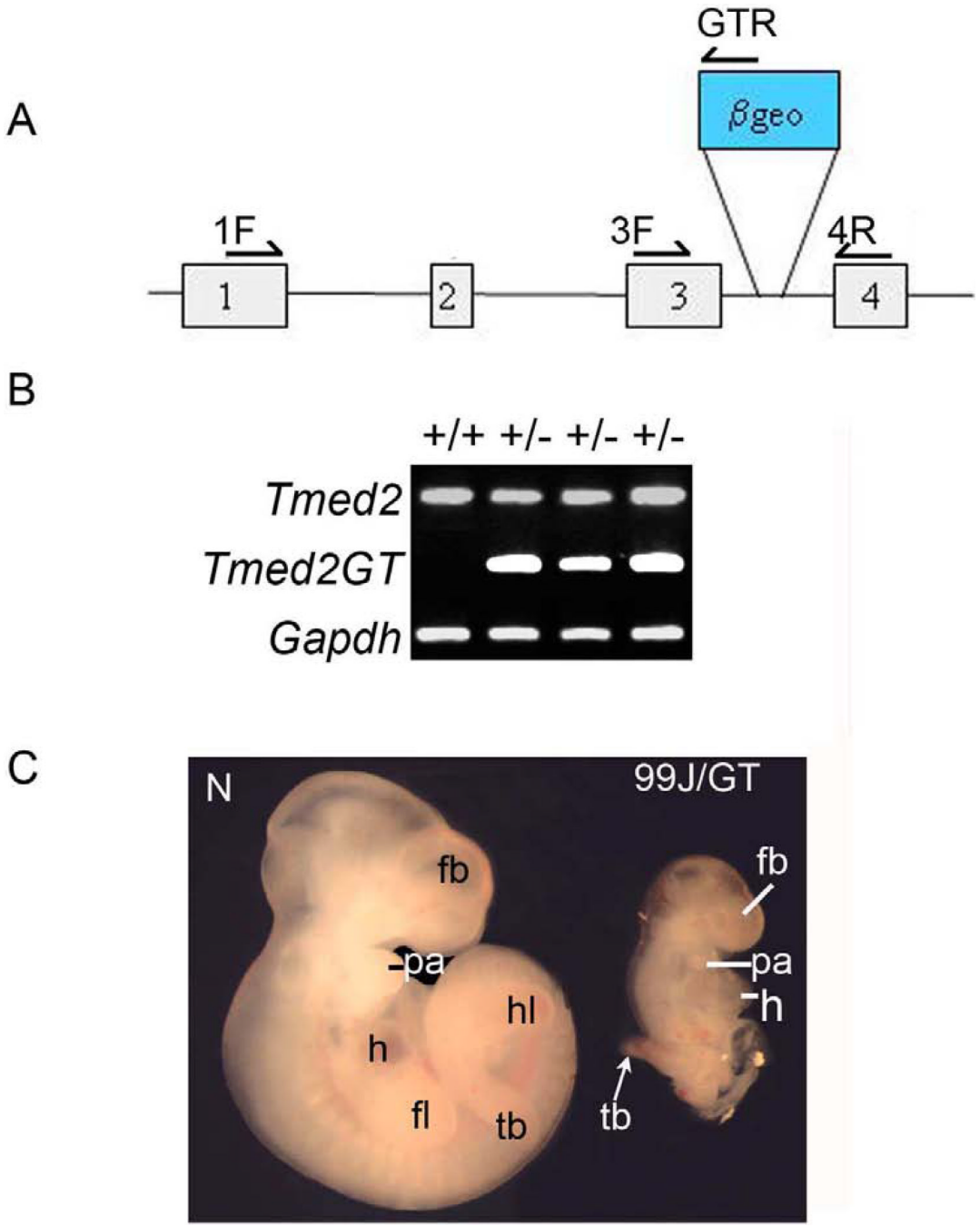

Figure 5. Gene trap insertion in *Tmed2* fails to complement the 99J mutation

(A) Schematic of the *Tmed2* genomic locus depicting insertion of the *β-geo* gene trap cassette in the third intron. (**B**) The fused *Tmed2* and *β-geo* transcript generated in the PST809 cell line was detected by RT-PCR with primers in *Tmed2* and the *β-geo* cassette. Primers 1F + 4R amplified the expected *Tmed2* transcript in wild type and $Tmed2^{GT}$ heterozygous embryos. In wild-type embryos, primers 3F + GTR did not generate any product (first lane). However, these same primers amplified the fused *Tmed2βgeo* transcript in heterozygous embryos. *Gapdh* was used as a positive control. (**C**) Representative images of E10.5 wild type and *99J/GT* trans-heterozygous embryos. The $Tmed2^{GT/99J}$ trans-heterozygous mutant embryo (right) is smaller than its normal littermate (left), and has relatively normal anterior development with evident

forebrain (fb) and pharyngeal arches (pa); however, similar to that observed in 99J homozygous mutant embryos, the heart (h) is unlooped and the posterior tail bud (tb) is reduced in size.

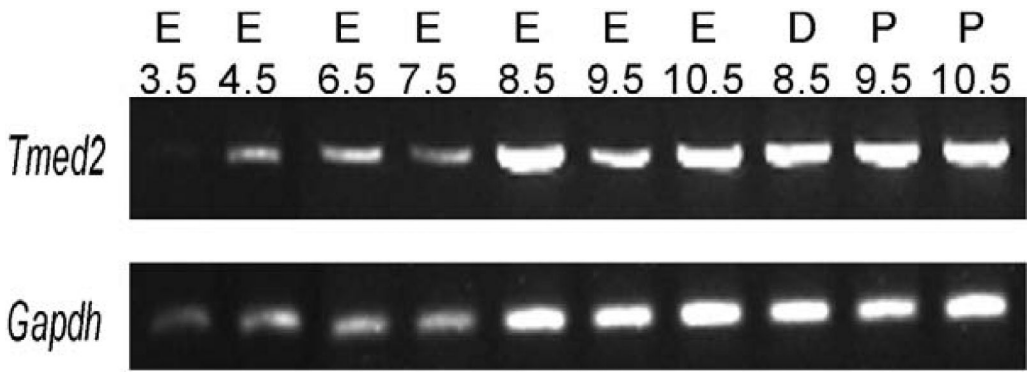

Figure 6. *Tmed2* is expressed throughout mouse embryonic development

RT-PCR showing the presence of the *Tmed2* as well as *Gapdh* transcripts in E3.5–E10.5 wild type embryos (E). *Tmed2* is also expressed in E8.5 deciduas (D) and E9.5 – E10.5 placentas (P).

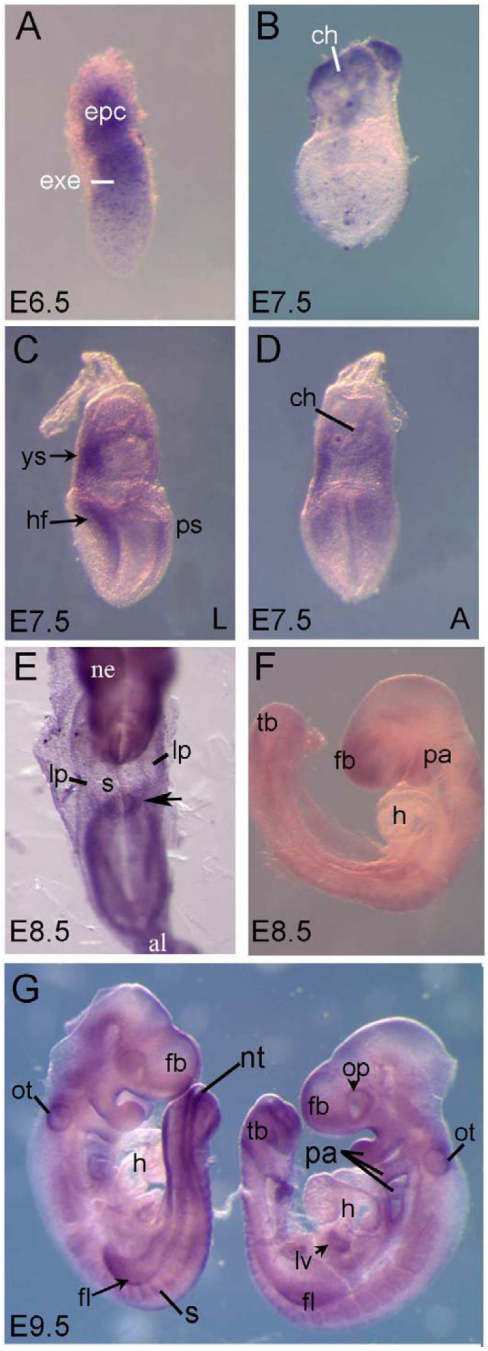

Figure 7. *Tmed2* expression during embryonic development

Representative images of wild type embryos after wholemount *in situ* hybridization with an antisense riboprobe to *Tmed2*. (**A**) Lateral view of an E6.5 embryo; *Tmed2* is expressed in the ectoplacental cone (epc) and the extraembryonic ectoderm (exe). (**B**) Lateral view of a mid-streak embryo; *Tmed2* is expressed in the chorion (ch). Lateral (**C**) and anterior (**D**) views of an early headfold stage embryo; *Tmed2* is expressed in the chorion (ch), yolk sac (ys), anterior mesoderm, and the proximal portion of the primitive streak. (**E)** Dorsal view of a representative E8.5 embryo; *Tmed2* is broadly expressed with high levels found in neural epithelium (ne), the peri-nodal region (arrow), presomitic mesoderm, tailbud and allantois (al); expression was low in the lateral plate (lp) and somites (s) and not found in the midline. (**F**) Lateral view of a

representative E8.5 embryo; *Tmed2* expression is highest in the forebrain (fb), pharyngeal arch (pa) and tail bud (tb). No expression was detected in heart (h). (**G**) Representative images of the right and left side of two E9.5 embryos showing high levels of *Tmed2* expression in tail bud (tb), pharyngeal arches (pa), otic vesicle (ot), forelimb bud (fl), liver anlage (lv), neural tube (nt), and optic vesicle (op).

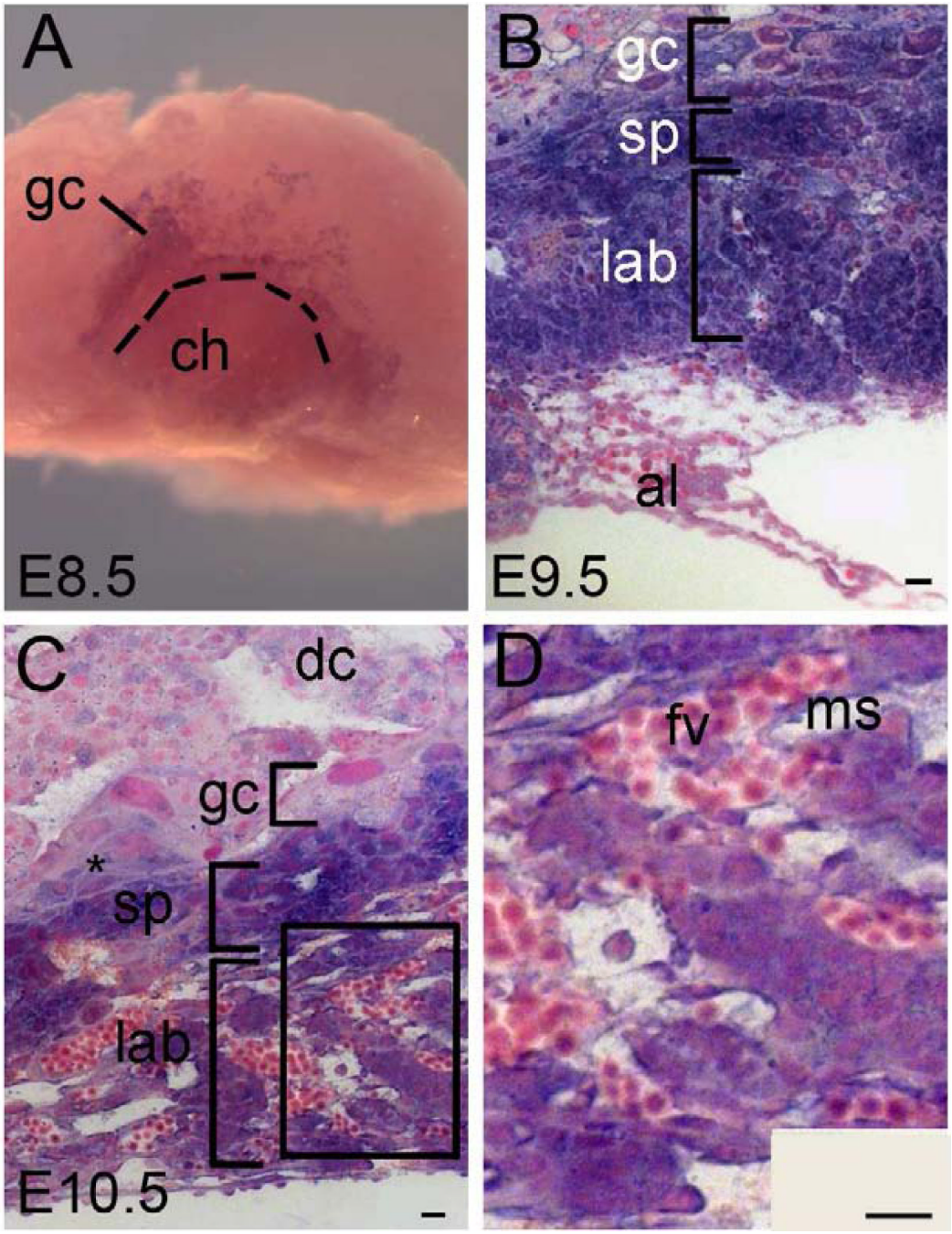

Figure 8. Expression of *Tmed2* during placental development

Representative images of wild type decidua (**A**) and placentas (**B, C, D**) after wholemount (**A**) and section (**B, C, D**) *in situ* hybridization with an antisense *Tmed2* riboprobe. (**A**) In an E8.5 decidua *Tmed2* is expressed in the chorion (ch) and giant cells (gc). (**B**) *Tmed2* is expressed throughout the placenta with the exception of the allantois. (**C**) *Tmed2* is expressed throughout the cells in the labyrinth layer (lab), as well as in the spongiotrophoblast (sp) and in a subset of giant cells (* and gc). *Tmed2* expression is also detected in a subset of cells in the maternal decidua (dc). No signal was detected with the sense probe (not shown) (**D**) Higher magnification view of boxed region in (**C**). Scale bars = 20 μm.

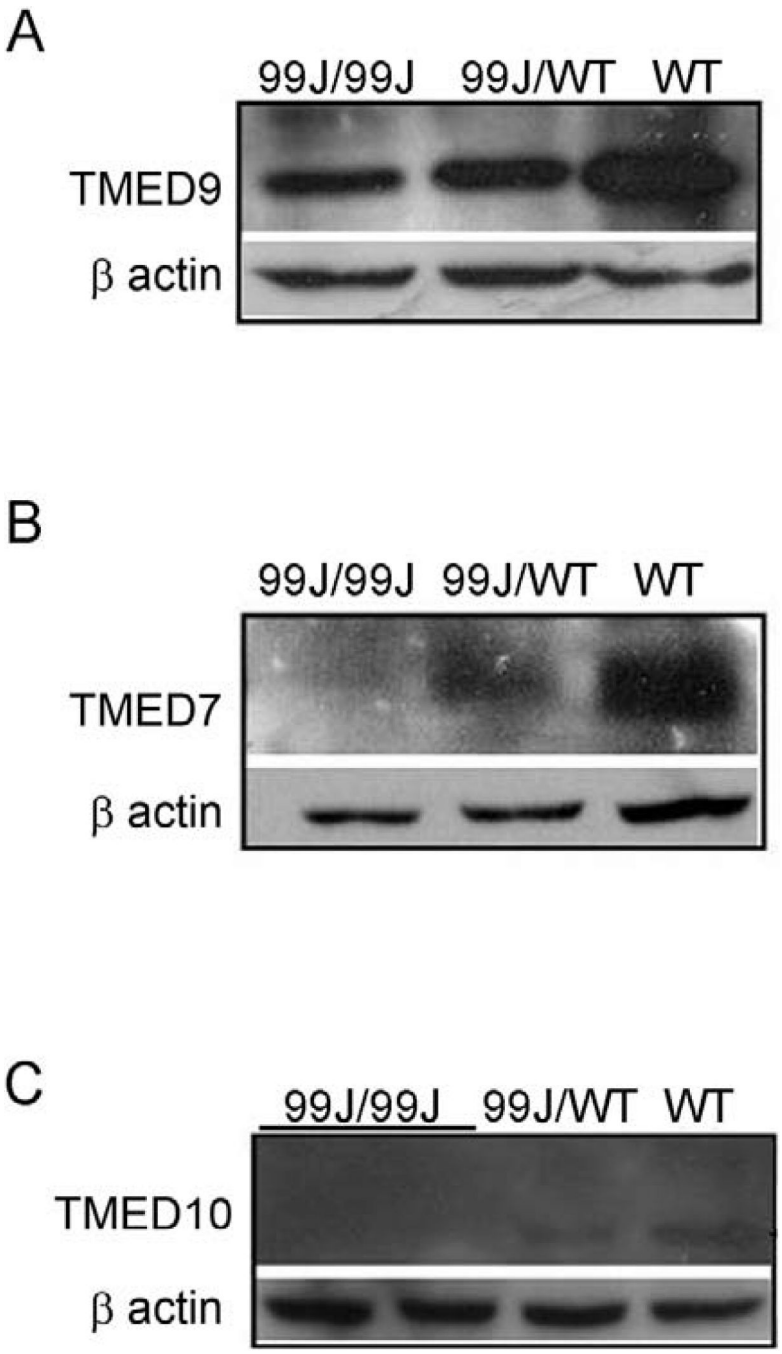

Figure 9. TMED2 is required for normal expression of TMED7, TMED9 and TMED10 at E9.5 and E10.5

(**A)** TMED9 is detected at reduced levels in 99J heterozygous and homozygous mutant embryos at E9.5. **(B)** At E9.5 TMED7 is present at reduced levels in 99J heterozygous embryos but is undetectable in 99J homozygous mutant embryos. (**C)** At E10.5 embryos, TMED10 is expressed at reduced levels in 99J heterozygous embryos but is undetectable in 99J homozygous mutant embryos. (**A-C)** β-actin was used as a loading control.

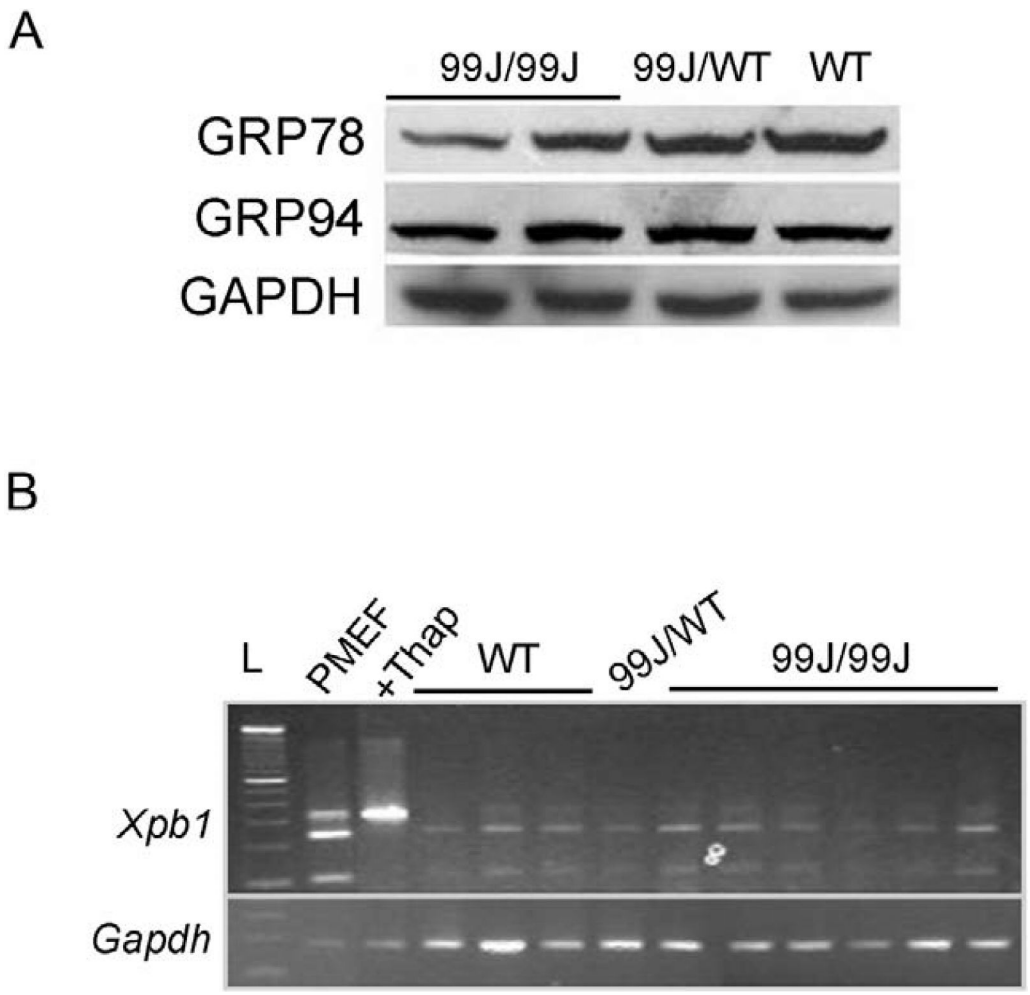

Figure 10. 99J homozygous mutant embryos do not show increased levels of ER stress-associated proteins

(**A**) No difference was detected in the levels of the ER resident proteins GRP78 and GRP94 in 2 different pools of 99J homozygous mutant, 99J heterozygous, and wild type embryos at E10.5. (**B)** RT-PCR showing the presence of un-spliced *Xbp1* as two bands of 240 and 110bp in unstressed PMEF cells, wild type, 99J heterozygous and 99J homozygous mutant embryos. A single 350 bp band representing spliced *Xbp1* is detected in PMEFs after stress with thapsigargin. The *Gapdh* transcript was also detected in all samples.

Table 1

Genotype distribution of embryos collected between E7.5 and E12.5 from mating of 99J carrier X 99J carrier

The number of embryos that genotyped as 99J homozygote mutant is in parenthesis.

Embryonic days of Development (E)	Phenotypically Normal Observed (99J homozygous mutant)	Phenotypically Abnormal Observed (99J homozygous mutant)
E7.5	13 (4)	0
E8.5	44 (1)	28 (20)[!]
E9.5	100	58 (48)[^]
E10.5	63	45 (35)[*]
E11.5	20	8 (4)[#]
E12.5	39	11 (4)[o]
Total	279 (5)	150 (111)

[!] 2 abnormal embryos had a recombination event between D5MIT65 and D5MIT213, 3 abnormal embryos were heterozygous, 1 abnormal embryo was wild type and 2 abnormal embryos were not typed

[^] 5 of the homozygous mutant embryos were dead, 4 abnormal embryos had a recombination event between D5MIT65 and D5MIT213, 4 abnormal embryos were heterozygous, and 2 embryos were not genotyped.

[*] 2 99J homozygous mutant and 1 99J heterozygous embryos were dead, 1 abnormal embryo had a recombination event between D5MIT65 and D5MIT213, 6 abnormal embryos were 99J heterozygous and 2 embryos were not typed

[#] All abnormal embryos were found dead, 2 were 99J heterozygous and 2 had a recombination event between D5MIT65 and D5MIT213.

[o] All abnormal embryos were dead, 1 embryo was 99J heterozygous and DNA could not be collected from 6 embryos.

Table 1B

The distribution of *99J* homozygous mutant embryos with right (R), or left (L) looping, or malformed (M) hearts in 5 99J intercross dissected at E10.5. Normal embryos had rightward looping heart in these litters. (n= 51)

	R	L	M
99J -/-	3	7	3
99J +/- or +/+	38	0	0

Table 2
Somite distribution in 99J homozygous mutant embryos at E8.5 and E9.5

99J homozygous mutant embryos were delayed and had fewer somites than wild type littermates at E8.5 and E9.5.

Age Genotype	0-2	3-15	16+
E8.5* 99J homozygous mutant	95% (n=20/21)	5 % (n=1/21)	
E8.5 Wild type	9 % (n= 1/11)	91 % (n=10/11)	
E9.5# 99J homozygous mutant	21% (n=9/43)	79 % (n=34/43)	
E9.5 Wild type	0	11 % (n-2/19)	89 % (n=14/19)

* $t(30) = 5.65$, $p<0.0001$

$t(61) = 14.1$ $p<0.0001$

Table 3
Summary of the analysis of the candidate genes in the 99J minimal region

Mutations in 4 genes did not resemble the 99J homozygous mutant phenotype (*). 3 genes were not expressed in normal or mutant embryos (N= not expressed, Y= expressed). 3 genes including *Tmed2* (Yellow) were expressed (E) in both the embryos and placentas (P) at E9.5 (Green). A single mutation was identified in the signal sequence of *Tmed2* (Y= mutation present, N= no mutation identified).

Gene Name	Expressed in normal and mutant embryos by RT-PCR analysis	Expressed in embryos or placentas by wholemount *in situ* hybridization analysis	Mutations in the gene sequence
Interleukin 31	N		N
B3gnt4	Y	E	N
Diablo*			N
Vsp37 b	Y	E	N
Rsn*		E	N
Zcchc8	Y	E	N
1500011J06Rik	Y		N
Kntc1	Y	E	N
Gpr109b	Y		N
Gpr81	N		N
Denr	Y	E	N
Abcb9	Y	E	N
Hip1r*			N
5730405M13Rik	Y	E	N
Arl6ip4	Y	E	N
Pitpnm2*			N
Mphosph9	Y		N
2810006K23Rik	Y	E	N
NM_013812.2	N		N
Sbno1	Y	E	N
2410195B05Rik (set 8)	Y	E	N
BC003324	Y	E	N
6330548G22Rik	Y	E	N
2900002H16Rik	Y	E	N
Tmed2	Y	E, P	Y
Ddx55	Y		N
Eif2b1	Y	E, P	N
Gtf2h3	Y	E	N
4432405B04Rik	Y	E	N
Atp6v0a2	Y		N
Dnahc10	Y	E	N
D5Bwg0834e	Y	E, P	N
D930038J03Rik	Y	E	N

Gene Name	Expressed in normal and mutant embryos by RT-PCR analysis	Expressed in embryos or placentas by wholemount *in situ* hybridization analysis	Mutations in the gene sequence
3110032G18Rik (Cfm2)	Y	E	N
Ncor2	Y	E	N